

# The role of pre-existing heterogeneities in materials under shock and spall

Cite as: Appl. Phys. Rev. **9**, 011305 (2022); <https://doi.org/10.1063/5.0053693>

Submitted: 09 April 2021 • Accepted: 27 August 2021 • Published Online: 19 January 2022

R. M. Flanagan,  S. J. Fensin and  M. A. Meyers

## COLLECTIONS

 This paper was selected as Featured



View Online



Export Citation



CrossMark

## ARTICLES YOU MAY BE INTERESTED IN

[Quantum emitters in 2D materials: Emitter engineering, photophysics, and integration in photonic nanostructures](#)

Applied Physics Reviews **9**, 011306 (2022); <https://doi.org/10.1063/5.0072091>

[Large unidirectional spin Hall and Rashba–Edelstein magnetoresistance in topological insulator/magnetic insulator heterostructures](#)

Applied Physics Reviews **9**, 011406 (2022); <https://doi.org/10.1063/5.0073976>

[Efficient and controllable magnetization switching induced by intermixing-enhanced bulk spin–orbit torque in ferromagnetic multilayers](#)

Applied Physics Reviews **9**, 011407 (2022); <https://doi.org/10.1063/5.0067348>



Applied Physics  
Reviews

Read. Cite. Publish. Repeat.

**19.162**  
2020 IMPACT FACTOR\*

# The role of pre-existing heterogeneities in materials under shock and spall

Cite as: Appl. Phys. Rev. **9**, 011305 (2022); doi: [10.1063/5.0053693](https://doi.org/10.1063/5.0053693)

Submitted: 9 April 2021 · Accepted: 27 August 2021 ·

Published Online: 19 January 2022



View Online



Export Citation



CrossMark

R. M. Flanagan,<sup>1</sup> S. J. Fensin,<sup>2</sup>  and M. A. Meyers<sup>1,a)</sup> 

## AFFILIATIONS

<sup>1</sup>University of California San Diego, La Jolla, California 92093, USA

<sup>2</sup>Los Alamos National Laboratory, Los Alamos, New Mexico 87545, USA

<sup>a)</sup>Author to whom correspondence should be addressed: [mameyers@ucsd.edu](mailto:mameyers@ucsd.edu)

## ABSTRACT

There has been a challenge for many decades to understand how heterogeneities influence the behavior of materials under shock loading, eventually leading to spall formation and failure. Experimental, analytical, and computational techniques have matured to the point where systematic studies of materials with complex microstructures under shock loading and the associated failure mechanisms are feasible. This is enabled by more accurate diagnostics as well as characterization methods. As interest in complex materials grows, understanding and predicting the role of heterogeneities in determining the dynamic behavior becomes crucial. Early computational studies, hydrocodes, in particular, historically preclude any irregularities in the form of defects and impurities in the material microstructure for the sake of simplification and to retain the hydrodynamic conservation equations. Contemporary computational methods, notably molecular dynamics simulations, can overcome this limitation by incorporating inhomogeneities albeit at a much lower length and time scale. This review discusses literature that has focused on investigating the role of various imperfections in the shock and spall behavior, emphasizing mainly heterogeneities such as second-phase particles, inclusions, and voids under both shock compression and release. Pre-existing defects are found in most engineering materials, ranging from thermodynamically necessary vacancies, to interstitial and dislocation, to microstructural features such as inclusions, second phase particles, voids, grain boundaries, and triple junctions. This literature review explores the interaction of these heterogeneities under shock loading during compression and release. Systematic characterization of material heterogeneities before and after shock loading, along with direct measurements of Hugoniot elastic limit and spall strength, allows for more generalized theories to be formulated. Continuous improvement toward time-resolved, *in situ* experimental data strengthens the ability to elucidate upon results gathered from simulations and analytical models, thus improving the overall ability to understand and predict how materials behave under dynamic loading.

Published under an exclusive license by AIP Publishing. <https://doi.org/10.1063/5.0053693>

## TABLE OF CONTENTS

I. INTRODUCTION .....	1
II. CRYSTAL ORIENTATION EFFECTS .....	2
III. POLYCRYSTALLINITY EFFECTS .....	3
IV. PRE-EXISTING HETEROGENEITIES AND SHOCK. .	8
A. Inclusions: Second-phase particles, precipitates, and bubbles .....	8
B. Voids .....	17
C. Porous materials .....	20
V. DISCUSSION .....	25
VI. CONCLUSIONS .....	27
ACKNOWLEDGMENTS .....	27
AUTHOR DECLARATIONS .....	28

## I. INTRODUCTION

Understanding and predicting the shock wave behavior of materials continues to be of great interest due its importance in many

applications. As humans collectively work toward traveling beyond our own moon, building nuclear fusion reactors, and developing faster means of transportation, among a plethora of other technological advancements, these endeavors expose materials to increasingly extreme environments. As such, in the case of collisions and impacts, the dynamic behavior of materials is crucial to understanding the life-cycle of the components in these ever-evolving technologies to ensure their longevity.

Material behavior under shock loading has fascinated researchers since the 1800s. Originally developed for fluids, the theory of shock was extended to solids and became particularly relevant during World War II when researchers began rigorously exploring the strength and failure mechanisms of solids. A material under shock loading experiences several stages of deformation as shown in Fig. 1. First, as the material experiences the initial impact, an elastic precursor [(A) and (B) in Fig. 1] travels ahead of the plastic wave [(C) in Fig. 1] where the stress generated by the shockwave exceeds the Hugoniot elastic

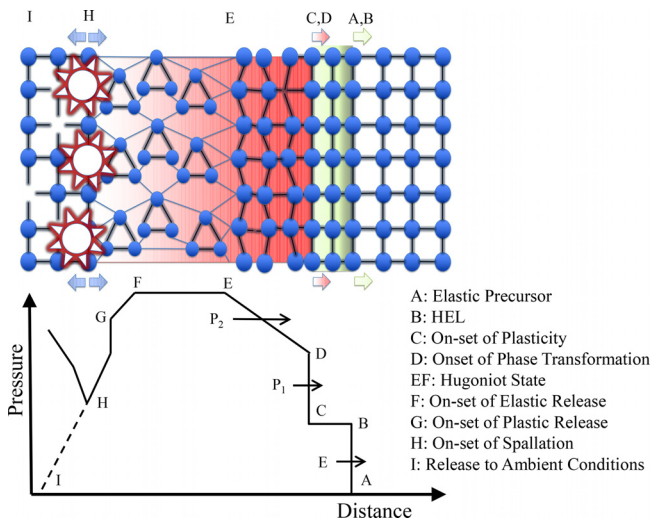


**FIG. 1.** A simplified rendering of the shock compression and release in a crystalline material. The shock wave has a two-wave structure, where the elastic precursor [(A) and (B)] is followed by the plastic wave (C) when the pressure exceeds the Hugoniot elastic limit (HEL). Some materials may undergo phase changes as they are rapidly compressed (D), while deformation-induced defects are generated throughout the Hugoniot state [(E) and (F)]. As the shock front reaches the rear free surface, depending on the loading conditions, it undergoes spallation (H) or release to ambient conditions (I). Reproduced with permission from Williams, "Structure-property relationships under extreme dynamic environments: Shock recovery experiments," *Synthesis SEM Lectures on Experimental Mechanics* (Morgan and Claypool, 2019). Copyright 2019 Morgan and Claypool Publishers.

limit (HEL). Some materials may undergo a phase transition [(D) in Fig. 1], and once the material reaches the Hugoniot state [(E) and (F) in Fig. 1], dislocations, twins, cracks, and other defects are generated. The primary research interest during this phase of shock, which we refer to as compression, have centered around the effect of pulse shape, dwell time, and elastic-plastic wave structure,<sup>1,2</sup> on the ensuing deformation mechanisms such as slip, twinning,<sup>3</sup> and phase transformations.<sup>4</sup> The compression stage of shock has been reviewed extensively by Bourne *et al.*,<sup>5</sup> who broke down the steps of compression into the formation of defects, noting that the "hierarchy of defect generation" depends on several factors, such as the point at which plastic flow begins, kinetics of defect formation for a specific material, temperature dependence, atomic packing, and, notably, initial defect concentration.

When the shock front reaches the rear free surface of a target, it is reflected in the form of release pulses that propagate through the material annihilating the pre-existing defects from the shock and also generating further microstructural defects,<sup>6</sup> which include dislocations, twins, and phase changes.<sup>3,7</sup> A significantly strong shock generates release pulses whose interaction induces triaxial tensile pressure and the nucleation of voids [(H) in Fig. 1], while other loading conditions allow for release back to ambient conditions [(I) in Fig. 1]. The region in which this interaction primarily occurs is known as the spall plane. Pre-existing defects such as grain boundaries, triple junctions, twins, stacking faults, and interfaces play an important role in the generation of voids, yet the ability to understand and predict the extent of the role each of these imperfections plays in void nucleation is challenging due to the spatial and temporal limits of current experimental methods.<sup>8</sup>

While diagnostics such as photon Doppler velocimetry (PDV) and velocity interferometry for any reflector (VISAR) are able to measure the velocity of the free surface as a function of time, allowing for analysis and measurement of the spall strength of the material,<sup>6,8–11</sup> previous research has shown that this information alone is not sufficient to understand damage morphology and evolution in materials.<sup>12–14</sup> There are multiple cases where the spall strength calculated from the velocity-time information is similar but the damage profile is completely different.<sup>13,14</sup> At the final stage, voids grow and coalesce, leading to the onset of complete failure. While access to powerful x-rays at the dynamic compression sector of Argonne National Laboratory and Linac Coherent Light Source along with other international facilities is becoming more available to obtain phase contrast imaging or *in situ* diffraction data, the most common method used to understand damage formation and evolution remains sample recovery coupled with postmortem characterization of spalled samples.<sup>9,11,15</sup> The straightforward nature of these spall experiments has made them a common way of studying dynamic fracture, but conflicting results of spall strength have been reported, especially in heterogeneous materials, because there is no direct way to measure the tensile stress within the material *in situ*.<sup>16</sup> Much work on pre-existing defects has focused on spall, but as *in situ* methodologies evolve, future studies will be better-equipped to address both compression and spallation.

In general, the response of a material to an applied shock is dependent not only on its microstructure but also on how the loading parameters like pulse duration, shape, and tensile strain rate couple with this microstructure.<sup>17</sup> In order to decouple these two phenomena, it is imperative to simplify the problem by initially studying simpler microstructures. In fact, perhaps due to this argument, the majority of the work in the field of shock physics has focused on single element materials like Cu, Ta, and Al without any heterogeneities or impurities.<sup>5,18–22</sup> There are a handful of studies that have, in a systematic manner, added heterogeneities to the materials and investigated their dynamic response;<sup>13,20,23–27</sup> these will be discussed later in the review.

The goal of this paper is to explore and evaluate existing literature describing the role of material defects and heterogeneities in the shock and spall response of metals and nonreactive materials. Studies have traditionally neglected the role of these heterogeneities during shock; for experiments, this is attributed to a combination of diagnostic difficulties and interest in other behaviors for materials under shock, while simulations must balance spatiotemporal resolution with computational power [for example, grain boundaries are simulated as either nanocrystalline materials or bicrystals in molecular dynamics (MD) simulations]. As interest in more complex materials grows, it is crucial to include heterogeneities to fully develop and predict material performance under shock loading. While there is a myriad of material imperfections, including vacancies, interstitials, dislocations, and grain boundaries, in this paper, heterogeneities refer specifically to pre-existing voids, bubbles, second phase particles, and other inclusions. Throughout this literature review, we evaluate the trends and themes observed regarding how the aforementioned heterogeneities alter the shock and spall behavior, both experimentally and computationally, when possible.

## II. CRYSTAL ORIENTATION EFFECTS

The simplest microstructures to study are single crystals. The majority of work in this area has focused on understanding the effect

of crystal orientation, tensile strain rate, pulse shape, and/or dwell time on the dynamic behavior of these simple materials. Face-centered cubic (FCC) materials have been extensively studied, with aluminum and copper being favored model materials. Kanel *et al.*<sup>28</sup> found that the spall strength of single crystal aluminum increased as a function of tensile strain rate. Gas gun experiments by Chen *et al.*<sup>26</sup> on single crystal aluminum, oriented along the [100] and [111] directions, suggested an orientation dependence of the spall strength with [100] orientation having the higher spall strength than [111]. Although the difference was attributed to the fact that while the [100] crystals were 99.999% pure, the [111] crystal had small amounts of impurities like Si, Fe, B, and P. As a follow-up to the Al study performed by Chen *et al.*,<sup>26</sup> Owen *et al.*<sup>29</sup> utilized plate impact experiments to better understand the spall behavior of [100], [110], and [111] Al, finding that the spall strength and the elastic–plastic transition stress (also termed the Hugoniot elastic limit or HEL) is largest for the [111] orientation, followed by the [110] and [100] orientations. Results from Owen *et al.*<sup>29</sup> were contrary to those of Chen *et al.*<sup>26</sup> and were recently elaborated upon by Millett *et al.*,<sup>30</sup> who agreed with the work of the latter. Gas gun experiments by Millett *et al.*<sup>30</sup> on single crystal Al demonstrate a dependence on orientation for post-shock hardening, with [100] orientation demonstrating the most hardening, followed by [110] and [111]. This orientation dependence is associated with the number of available active slip systems as estimated by the Schmidt factor for FCC materials.

Contrary to trends in Al, the dependence of spall strength is different in copper. Work by Minich *et al.*<sup>20</sup> demonstrated that the [100] orientation in single-crystal copper had the highest spall strength, followed by [110] and [111], likening this phenomenon to the availability of active slip systems relative to their different strain hardening rates. A later publication by Turley *et al.*<sup>31</sup> reiterated that the [100] direction did indeed have a higher spall strength, also revealing that the [100] direction exhibited a more rapid spall formation compared to other orientations. This paper also highlighted tensile peak stress and tensile strain rate as key parameters that affect spall strength. It is generally difficult to change only one parameter during shock loading, such as tensile strain rate, in a systematic manner without affecting other parameters like tensile stress or pulse duration, but this goal was successfully achievable by this goal. These experimental studies are also complemented by simulation work to understand the dependence of spall strength on orientation. Specifically, molecular dynamics (MD) simulations by Dongare *et al.*<sup>32</sup> on single crystal Cu found that voids nucleate at stacking fault intersections in the spall plane in two stages, first nucleating rapidly and then slowly coalescing. This result is reaffirmed by Mackenchery *et al.*<sup>33</sup> who utilized MD simulations to demonstrate that single crystal Cu deforms via twinning partials and Shockley partials under shock loading, and the nucleation of voids occurs at stacking fault intersections. Hence, deformation mechanisms, as they change with orientation, can have a significant effect on spall strength.

The crystalline structure itself presents another facet for understanding and predicting shock behavior. Body centered cubic (BCC) metals exhibit both the lowest density of mobile dislocations and the slowest rise time for shock, while Face Centered Cubic (FCC) metals have a much more rapid rise time and a larger number of available deformation systems. Low symmetry structures like hexagonal close packed (HCP) metals have even less available slip systems than BCC

or FCC metals due to the symmetry of their structure, and texture can also play an important role in their deformation behavior.<sup>5</sup> In high stacking fault energy materials, dislocation networks are often tangled due to strain hardening; conversely, low stacking fault energy materials such as Ta develop long screw dislocations throughout the material due to a decrease in shear stress behind the shock front.<sup>34</sup> Stacking fault energy also plays a role in deformation via twinning, which occurs when stacking faults advance through material in a seemingly coordinated manner.

There is a critical shear stress at which twinning can occur, but it is dependent on the material as well as its dislocation density and texture.<sup>35,36</sup> To investigate the orientation dependence of twinning in tantalum, McNaney *et al.*<sup>37</sup> utilized electron back-scattered diffraction (EBSD) on samples that were shocked along the [011] direction, which demonstrated significant twinning, while [001] orientations showed nearly no twinning. Similarly, Pang *et al.*<sup>38</sup> explored the shock behavior of tantalum and found that shock along the [011] and [111] directions induced twinning as a major deformation mechanism, whereas the [001] orientation exhibited an insignificant amount of twinning behind the shock front. The [001] orientation also exhibited a greater HEL and spall strength compared to the [011] and [111] orientations, possibly suggesting that twinning reduces the spall strength by acting as location for void nucleation, with both the twin boundary and the crystal with a weaker orientation acting as void nucleation sites. Lu *et al.*<sup>39</sup> estimated the pressure at which deformation transitions from slip to twinning to be approximately 32–43 GPa regardless of orientation. Contrary to these studies, work by Whiteman *et al.*<sup>40</sup> and Hahn *et al.*<sup>41</sup> suggested that the spall strength is actually the lowest along the [001] direction. An *et al.*<sup>42</sup> note that this is likely due to a change in twin density, which is dependent on strain rate and pulse shape, which determines spall strength. However, it is important to note that all orientations showed twin nucleation and growth in the modeling work by An *et al.*,<sup>42</sup> suggesting that once the threshold stress for deformation to be twin based is crossed, orientations can have varying amounts of twin density. Studies on Mg by Renganathan *et al.*<sup>43</sup> via experiments and direct numerical simulations demonstrated similar results to An *et al.*,<sup>42</sup> with orientation playing a clear role in deformation via slip vs twinning. Twinning may also occur at different stages of shock; for example, in magnesium, shock along the  $\langle a \rangle$ -axis generates compression twins that subsequently de-twin during release, while shock along the  $\langle c \rangle$ -axis forms twins only during release,<sup>7,44</sup> with pre-existing twins also serving as damage nucleation sites.<sup>45,46</sup> In general, while the processes by which deformation occurs have been probed anecdotally, with a variety of parameters able to influence whether slip or twinning is dominant and the interplay between deformation and material dynamic behavior, their effect on spall formation still remains underappreciated.

### III. POLYCRYSTALLINITY EFFECTS

As defects such as grain boundaries are added to the crystals, the orientation of the grains themselves becomes less important in dictating dynamic strength. Polycrystallinity also has a significant effect on spalling. Grain boundaries have been long-postulated to alter the spall behavior of a material, but simple parameters like boundary energy and excess volume have been found to not correlate with spall strength.<sup>47</sup> MD simulations of copper bi-crystals show that varying the orientation of both boundaries and grains can generate anisotropy

during both elastic and plastic deformation, leading to strong stress concentrations and differing spall strengths as a function of orientation.<sup>48</sup> Similar to the simulations, shock recovery experiments on copper bi-crystals reveal an orientation dependence of deformation twinning based on the deviatoric stress induced by the shock relative to the energetically favorable formation of Shockley partial dislocations.<sup>49</sup> The orientation of the grain boundaries with respect to the shock direction has also been shown to affect void nucleation at the boundaries. Specifically, boundaries oriented normal to the shock front were found to be ten times more likely to nucleate a void compared with boundaries oriented parallel to the loading direction due to differences in dissipation mechanisms for applied stress.<sup>50</sup> Void nucleation generally occurs at large inclusions, interfaces, grain boundaries and junctions, and vacancy complexes via dislocation loop emission depending on the applied stress. MD simulations by Zhang *et al.*<sup>51</sup> on  $\Sigma 5$  grain boundaries (low-angle grain boundaries) in a Cu bi-crystal indicate that partial dislocation loops nucleate and propagate from grain boundaries, while cracks tend to nucleate along the grain boundary plane, thus leading to brittle failure. Fortin *et al.*<sup>52</sup> performed flyer-plate impact experiments on Cu bi-crystals with a  $42^\circ$  misorientation, showing that the pulse duration and amplitudes during shock loading may alter the preference for intergranular or intragranular damage nucleation, while further work is under way; Fortin *et al.*<sup>52</sup> also hypothesized that damage kinetics likely accelerated at grain boundaries, hence the apparent preference for void nucleation and growth within grain boundaries.<sup>53</sup> MD simulations of  $\Sigma 11$  grain boundaries in Cu bi-crystals by Fensin *et al.*<sup>54</sup> emphasized the localized nature of plasticity at grain boundaries by showing that the amount of plastic deformation during shock loading is dissimilar for ordered and disordered grain boundaries with the same misorientation. For model cubic materials Cu and Ta, the sequence of void nucleation, growth, and coalescence differs due to the different availabilities of slip systems in each material; for Cu, voids were found to form along grain boundaries (preferably high-angle boundaries), while Ta mainly exhibited intragranular damage.<sup>55</sup> A systematic study of 74 tantalum bi-crystals by Chen *et al.*<sup>56</sup> to understand the role played by grain boundary structure during spallation showed that while there was no direct correlation between average grain boundary properties such as energy, excess volume, and spall strength, there was a correlation between grain boundary structure and spall strength. Specifically, a dependence of spall strength on the misorientation angle was identified, with spall strength being higher for grain boundaries whose normal direction was close to the [100], [111], and [112] directions. Further study of Ta bi-crystals via MD revealed that as the misorientation angle increased, there were transitions between void-nucleation-dominated failure and void-coalescence-dominated failure as well as slip-mediated deformation and twinning-mediated deformation.<sup>57</sup> Earlier experiments by Escobedo *et al.*<sup>58</sup> echoed these results, showing that  $\Sigma 1$  (low-angle grain boundaries) and  $\Sigma 3$  (coherent twin boundaries) in Cu are less likely to nucleate voids, implying that these particular boundaries are likely to be stronger. Such a trend was also observed by Peralta *et al.*<sup>59,60</sup> in Cu.

However, Nguyen *et al.*<sup>61</sup> suggested that misorientation is not sufficient for predicting the likelihood of intergranular spall failure, emphasizing the continuous progression of the role of grain boundaries. They conducted mesoscale calculations on polycrystals and concluded that elastic and plastic anisotropy alone accounted for

preferential failure at grain boundaries. Grain boundaries were modeled as perfectly bonded interfaces devoid of any weakening factors. They were able to compare the experimentally determined probability of localized damage (at grain boundaries) for different orientation relationships with their calculations. The incorporation of  $\Sigma 3$  coherent twin boundaries improved the agreement between experimental results (in blue) with computations (in yellow, with  $\Sigma 3$  boundaries). Figure 2 shows the juxtaposed results. The right-hand ordinate represents the experimental results, whereas the left-hand ordinate is the Bayesian conditional probability to find failure ( $\epsilon_f$ ) before an applied strain  $\epsilon_{app} = 0.2$  is reached. By incorporating  $\Sigma 3$  boundaries a good agreement is reached. Regardless, within the past decade, quantitative analyses have demonstrated a preference for failure at grain boundaries, as demonstrated in Fig. 3;<sup>62–64</sup> this highlights the role of dislocation emission as a mechanism for dissipation during void nucleation.<sup>63</sup>

Meyers<sup>65–67</sup> and Meyers and Carvalho<sup>68</sup> proposed that the shock front was affected by the polycrystallinity of the material and acquired an irregular configuration. This concept had been originally expressed in a qualitative manner in Meyers<sup>65</sup> doctoral dissertation and informally named “wavy wave” configuration [Fig. 4(a)]. These irregularities are due to differences in velocity between crystalline orientations, internal reflections, and other dispersive effects. Calculations were performed showing that the shock-front width increased with increasing grain size for the same travel distance. Figure 4(b) shows the dispersion of the shock front after the passage of the shock wave through 150 grains. Atomistic simulations of shock wave propagation in nanocrystals were carried out by Bringa *et al.*<sup>69</sup> and showed that the width of the wave front is indeed a function of grain size, pressure, and time. The atomistic calculations matched the analytical calculations of Meyers<sup>67</sup> and Meyers and Carvalho<sup>68</sup> for the width of the shock front for polycrystalline copper which, in turn, agree with measurements of Jones and Holland<sup>70</sup> in the microcrystalline regime. The simulations suggest that the effect of grain boundaries on the width of the wave front is small compared to the effect of anisotropy from crystal to

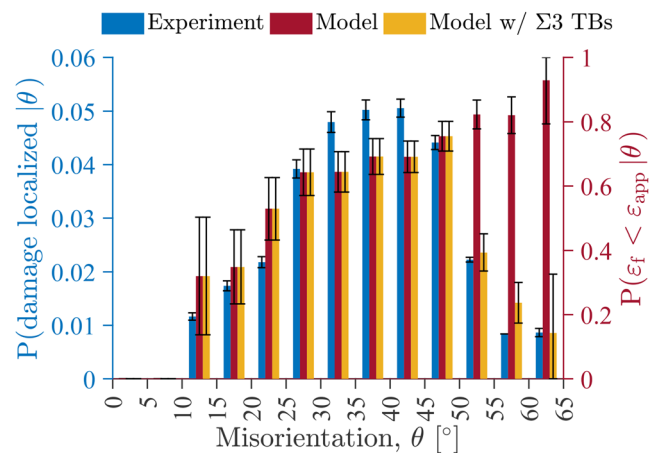


**FIG. 2.** Comparison of experimentally measured probability of damage along interfaces with mesoscopic computations for different misorientation angles varying from  $0^\circ$  to  $64^\circ$ . Reproduced with permission from Nguyen *et al.*, *Acta Mater.* **168**, 1–12 (2019). Copyright 2019 Elsevier.



FIG. 3. Spalling voids in copper forming preferentially at grain boundaries.

crystal. This is the reason why the continuum model by Meyers<sup>65–67</sup> was able to predict the front dispersion due to polycrystallinity. The dispersion of the wave calculated by MD, represented by the shock-front width normalized to the grain size,  $\Delta z/d$ , vs grain size, at three shock pressures (22, 34, and 47 GPa) is shown in Fig. 3(c). This shows that the normalized shock-front thickness decreases with increasing grain size and pressure, whereas the absolute (un-normalized) shock-front width decreases with decreasing grain size. The comparison of simulations, experimental measurements by Jones and Holland,<sup>70</sup> and analytical calculations by Meyers and Carvalho<sup>68</sup> is shown in Fig. 3(d). It can be seen that they all predict these irregularities. It should be noted that as the pressure is increased much beyond the HEL, these differences become irrelevant since the shock front becomes more homogeneous, which may be referred to as a hydrodynamic response.

In polycrystalline materials, the dynamic response can be altered by texture, grain size, and types of boundaries present.<sup>19</sup> In fact,

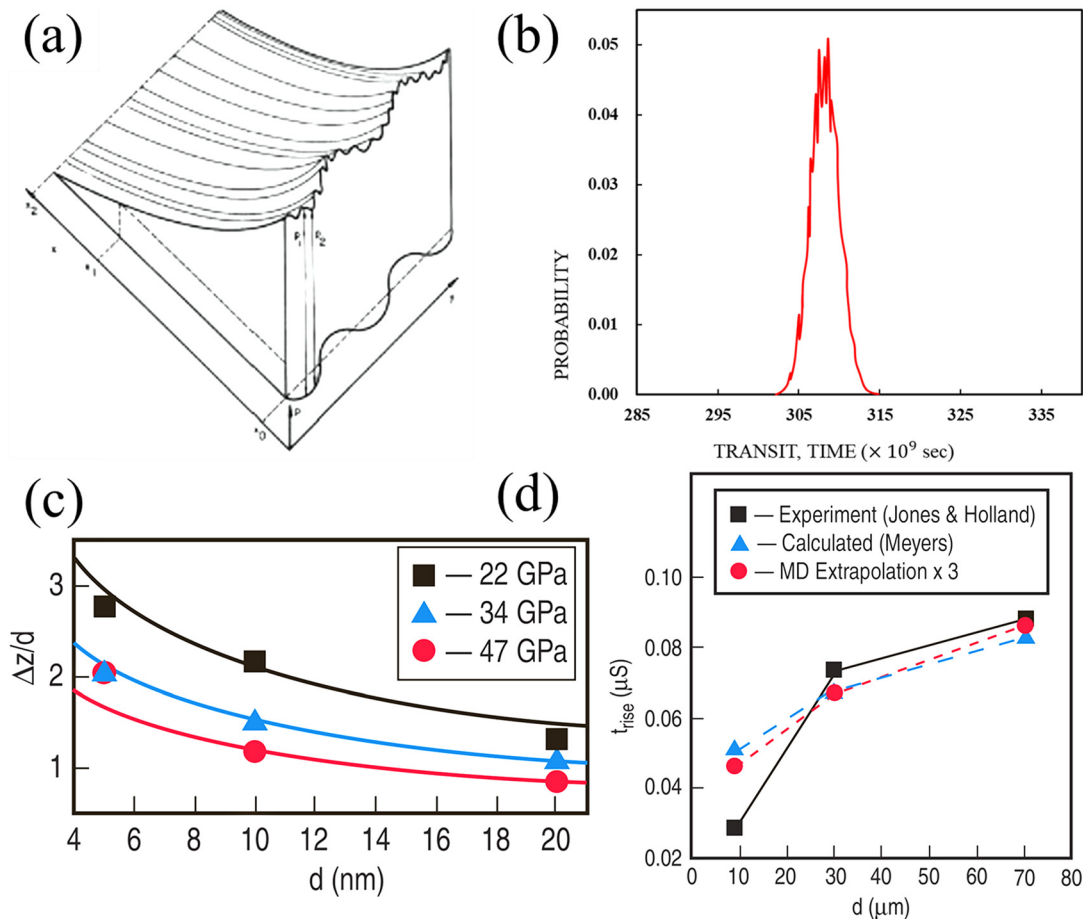


FIG. 4. Effect of polycrystallinity on shock-wave propagation: (a) qualitative "wavy wave" concept and (b) shock front variation due to the propagation through different grain orientations, each with a characteristic velocity. [Reproduced with permission from Meyers and Carvalho, *Mater. Sci. Eng.* **24**(1), 131–135 (1976). Copyright 1976 Elsevier.] Variation in front irregularity,  $\Delta z/d$  with grain size  $d$ ; [Reproduced with permission from Bringa *et al.*, *JOM* **57**, 9 (2005). Copyright 2005 Springer.] (d) Comparison of experimental, analytical calculations, and MD predictions (the latter, multiplied by 3) stress rise times with propagation distance. [Reproduced with permission from Nguen *et al.*, *Acta Mater.* **168**, 1–12 (1968). Copyright 1968 Elsevier.]

interest in polycrystalline materials has grown in the shock community in recent years due to observations which conflict with the well-known Hall–Petch relationship.<sup>71,72</sup> The relationship between spall strength and length scale was summarized by Meyers *et al.*,<sup>73</sup> and several studies have produced results contrary to the traditional Hall–Petch relation.<sup>20,58,62,74–78</sup> Minich *et al.*<sup>20</sup> postulated that the surface area of grain boundaries decreases as the grain size increases, which reduces the number of void nucleation sites and thus increases the spall strength, but asserted that transgranular void formation in finer-grained samples needs to be further examined. Localization of intergranular damage in Cu showed that grain boundaries with misorientations between 25° and 50° were preferred damage nucleation sites.<sup>59,62</sup> One potential resolution of conflicting results around the Hall–Petch formulation may be that the fraction of special grain boundaries, such as  $\Sigma 1$  and  $\Sigma 3$  in Cu that are mostly immune to void nucleation, influence the spall strength to such an extent that if the number of special boundaries is not controlled, a significant decrease in special boundaries with an increase in grain size would alter the number of potential nucleation sites.<sup>58</sup> While  $\Sigma 1$ ,  $\Sigma 3$ , and low angle grain boundaries may meet criteria for secondary slip, high angle grain boundaries and disordered grain boundaries develop stress concentrations due to dislocation pile ups, thus increasing their likelihood to be sites for failure.<sup>50,75,76,79</sup> This change in deformation mechanism due to a change in grain size can eventually alter the dynamic strength of a material. Brown *et al.*<sup>80</sup> noted that a decrease in spall strength of the bulk material diminished the localization of voids at grain boundaries since other damage nucleation sites in the spall plane can “compete” with grain boundaries. Escobedo *et al.*<sup>58</sup> attributed this to measurements taken during shock experiments in which complete failure is observed, where the interplay between many parameters and mechanisms plays an important role, thus suggesting that continued exploration of this field requires careful consideration of the phenomena of interest.

Reducing the grain size has been shown to drastically change the deformation mechanisms under shock loading. In general, nanocrystalline materials demonstrate a low-work hardening rate, decreased ductility, shear localization, and twinning, as reviewed by Meyers *et al.*<sup>81</sup> Tang *et al.*<sup>75</sup> found that during compression at strain rates of  $10^8$ – $10^9$  s<sup>-1</sup>, there is an inverse dependence of flow stress on grain size in nanocrystalline Ta, attributed to a decrease in grain boundary sliding and an increase in dislocation motion as grain size increases. Wilkerson and Ramesh<sup>82,83</sup> successfully derived a quantitative model applicable at very high strain rates, i.e.,  $10^4$  s<sup>-1</sup> and beyond, to define multiple regimes where (1) the Hall–Petch behavior is followed, (2) strength scales inversely to the Hall–Petch law, and (3) grain size no longer matter. For dynamic failure, a reduction in grain size has been found to be controversial as discussed above. MD simulations have been used to try to resolve these contradictory results further. Specifically, Bringa *et al.*<sup>84</sup> found voids to preferentially nucleate at grain boundaries in nanocrystalline Cu, which grow and coalesce, eventually elongating along the boundaries and acting as a crack. Additionally, grain-size dependent slip-twinning transition pressure has been identified via constitutive modeling and experiments on Ta<sup>39</sup> and observed via MD simulation.<sup>85</sup> A review of nanocrystalline materials under shock loading by Hahn *et al.*<sup>80</sup> thoroughly outlines recent findings in deformation in relation to grain size, particularly nanocrystalline materials and the prevalence of grain boundary sliding vs dislocation motion, as well as the critical size at which the traditional Hall–Petch slope turns over to become negative.<sup>86</sup>

While grain size is important in determining the dynamic strength of a material, the texture of the grains also matters. For example, forged Armco-iron showed an increase in spall strength in comparison to the same as-received material, approaching the strength of single crystal Fe, likely due to a dramatic decrease in the grain size and significant change in texture from the forging process (which elongates grains while reducing the size of inclusions).<sup>87</sup> Later experiments comparing pure rolled iron to annealed iron showed a greater HEL and a decreased spall strength for annealed Fe due to an increase in the number of sites available for void nucleation in the annealed material, likely due to the more equiaxed grain microstructure generated by annealing.<sup>88</sup> Earlier experiments found a similar trend for both annealed vanadium and tantalum, attributed to the effect of annealing, which generates a more homogeneous grain structure in comparison to rolled material.<sup>89</sup> Peralta *et al.*<sup>90</sup> examined the role of grain texture in polycrystalline copper, finding that columnar samples experience transgranular damage, while more equiaxed grains tended to nucleate intergranular damage; a noticeable difference in spall strength across grain boundaries due to anisotropy and impedance mismatch was also reported. Simulations of vapor-deposited and cold-rolled Al were also performed, emphasizing the importance of material heterogeneities due to differences in texture and its effect on wave profile;<sup>91</sup> plasticity modeling by Clayton<sup>92</sup> on tungsten heavy alloys also emphasized the importance of material phase and texture. An exemplary systematic study by Gray *et al.*<sup>93</sup> found that the dynamic response of the additively manufactured (AM) 316L stainless steel was altered based on the microstructure generated during the additive process. Specifically, three materials were studied: wrought 316L SS, AM-as-built 316L SS, and annealed AM-as-built 316L SS with microstructures varying from equiaxed to fine-scaled dendritic microstructure. This work showed that recrystallized AM 316L SS exhibited the highest spall strength and a typical spall plane at the region of peak tension, while the AM-as-built 316L SS tended to nucleate damage throughout the sample, outside regions of peak tensile load, likely due to the microstructure which seemingly alters the mechanism for damage nucleation.<sup>93</sup> A similar result, where a homogenized microstructure displayed a decreased spall strength, was also observed in an Mg alloy by Mallick *et al.*<sup>94</sup> By varying the processing of materials, it was shown that the nucleation, growth, and coalescence of damage are dependent on the grain size and texture; materials that undergo solid phase changes, particularly under shock loading, further complicate our understanding of deformation under shock loading.

Materials undergoing polymorphic transformations exhibit a three-wave structure under shock compression. When the stress exceeds the phase transformation value, a visible kink in their shock-wave profile due to phase changes can be observed.<sup>88,95</sup> The alpha-epsilon-alpha (bcc-hcp-bcc) phase transformation during shock in Fe plays an important role in determining its spall behavior as evidence of this phase change is found to be local to the spall surface in recovery experiments.<sup>96,97</sup> A multi-scale model of a generalized two-phase material shows that failure initiation sites are likely to be localized around the hard phase, while bands of soft phase intersect along directions of shear; there is a critical stress at which fracture initiation is dominated by the soft phase and is a function of the hard phase volume fraction as well as the contrast between mechanical properties of the materials.<sup>98</sup> Dual-phase stainless steel has a HEL similar to softer austenite, but the harder ferrite phase dominates the yield stress at

lower strain rates, with anisotropy and mismatch between these phases generating large shear deformations.<sup>99</sup> While dual phase stainless steel exhibited void nucleation at phase boundaries, Ti-6Al-4V exhibited void nucleation predominantly within the  $\alpha$  phase or at grain boundary triple points with higher differences in orientation, and a corresponding decrease in strength with an increase in the content of  $\alpha$  phase.<sup>100</sup> This is similar to behavior observed in dual-phase steels, where voids nucleate at phase boundaries and the HEL is dominated by the austenite phase.<sup>99</sup> All the above observations on the deformation behavior and the subsequent dynamic strength can be subsequently altered by the presence of heterogeneities. In fact, previous works have shown that void nucleation occurs hierarchically at inclusions, interfaces, grain boundaries and junctions, and vacancy complexes.<sup>101</sup> However, when heterogeneities are located at grain boundaries, this behavior will change again as will be discussed below.

In addition to the microstructure, it is important to also understand how the specific loading conditions such as pulse shape, duration, and strain rate couple with the microstructure. Koller *et al.*<sup>102</sup> observed a strong dependence of spall strength on loading and unloading shock profiles, as well as peak stress and tensile pulse duration, yet they note that further experiments are required to elucidate upon the damage processes (via second shock) and release time (via wave-shape-tailoring). A similar trend was seen in Al by Gray *et al.*,<sup>103</sup> which they attributed to the competition between shock hardening and work softening. Gray *et al.*<sup>103</sup> found a strong dependence of the spall strength on shock-wave profile for 316L stainless steel, with triangular-wave loading requiring twice the peak pressure of a square wave before incipient spall was observed, but no emphasis was placed on the defect characteristics of 316L stainless steel, likely due to the challenges in understanding deformation models, even in pure materials. MD simulations of copper showed that a compression pulse with a square shape vs one with a triangular shape shifts the damage from void nucleation to shear localization.<sup>104</sup> Experiments and hydrocode simulations of Cu demonstrate that strain rate and pulse shape were not found to alter the spall strength significantly.<sup>105</sup> Large scatter between peak stress and spall strength is prevalent throughout the literature,<sup>31</sup> but much of this work focuses on FCC materials. Conflicting reports of the role played by tensile strain rate and pulse shape have also been made for BCC materials. Jones *et al.*<sup>106</sup> found that strain rate and pulse shape do not alter the spall strength, as measured from the velocity-time information, for tantalum via gas gun experiments, but the total amount of damage in each sample was found to vary as a function of both peak stress and tensile strain-rate. Specifically, a larger quantity and size of voids was correlated with increased peak stress, while strain rate was found to alter damage evolution where a higher strain rate led to voids remaining in the nucleation and growth phase, while lower strain rates induced void coalescence. Conversely, as illustrated in Fig. 5, the spall strength increases with the tensile strain rate.<sup>11,107</sup> Similar trends have been realized for magnesium<sup>9</sup> and copper.<sup>31</sup> The complex interplay between spall strength, strain rate, and grain size in Ta is also illustrated, and the combination of present work and previous work plotted by Remington *et al.*<sup>11</sup> in Fig. 5 demonstrates the large amount of experiments needed to begin drawing conclusions regarding spall strength and the multitude of factors that alter it. An important recurring theme throughout the literature is the need for development of additional experimental *in situ* diagnostics to advance the capabilities of these shock experiments; improvements in both temporal and

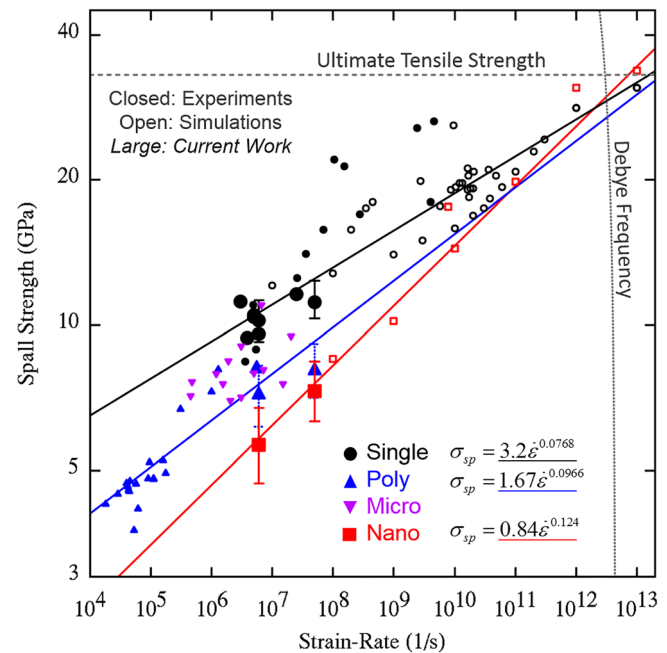


FIG. 5. Both computational and experimental results of Ta demonstrate an increase in spall strength with strain rate. The role of grain size is also summarized, with single crystal Ta being strongest until a strain rate of  $\sim 10^{11} \text{ s}^{-1}$ . Reproduced with permission from Remington *et al.*, *Acta Mater.* **158**, 313–329 (2018). Copyright 2018 Elsevier.

spatial resolution, as well as advancement and increased access to *in situ* diagnostics such x-ray diffraction and phase contrast imaging are ongoing. For example, measurements of elastic precursor decay have been linked to material strength during shock compression for metals containing point defects.<sup>108–110</sup> The decay of the elastic precursor has been successfully used to interrogate the internal structure; irregularities in the microstructure manifest themselves through variations in the rate of decay. 6061 aluminum alloys in different aging conditions, producing atomic clusters, GP1 zones, and GP2 zones were shown by Gray<sup>22</sup> to result in differences in the decay of the amplitude of the elastic precursor wave. This enabled the identification of changes in the mechanisms governing dislocation motion. For alpha brass, similar results were obtained.<sup>110</sup>

Another recurring theme throughout the field of shock is the influence of compressive and tensile strain rate on the dynamic behavior of materials. A 2012 review by Gray<sup>22</sup> concludes that the influence of strain rate is multifaceted. First, in low-stacking fault energy FCC metals, increasing strain rate produces more uniform dislocation distributions, which tend to be planar, lacking formation of discrete dislocation cells and increasing local misorientation. In high-stacking fault energy FCC metals, increasing strain rates leads to deformation-twin formation, while slip tends to be preferred at lower strain rates. Shock loading and increased strain rate correspond to an increase in dislocation jog, dislocation velocity, and therefore, point defect generation. The substructure of materials and the dislocations observed therein are heavily influenced by changes in strain rate and temperature<sup>111</sup> although it is clear that future studies ought to consider the entire loading path of a material rather than only free surface

measurements as the field grows.<sup>106</sup> The importance of loading path was exemplified by Bourne *et al.*<sup>112</sup> via gas gun experiments whose results correlated hardening of a material substructure with an increase in spall strength, implying that the processes under shock compression somehow relate to the processes underlying spallation. While there is significant work to be done to generalize a model for tensile failure, performing systematic and thorough studies of materials under shock loading will certainly aid in the process of creating and validating such a model.

#### IV. PRE-EXISTING HETEROGENEITIES AND SHOCK

The shock and spall behavior of materials has been reviewed extensively, but a major recurring theme is the lack of systematic studies specifically addressing the effect of pre-existing heterogeneities on this behavior.<sup>5,8,9,18,19,22,86,111,113</sup> Much of the work in this field has explored experimental and modeling tools to eventually be able to predict material failure under extreme conditions. Reviews published as recently as 2020 emphasize that the role of second phase particles and inclusions is understudied due to the challenges of isolating such microstructural parameters via experiments.<sup>9</sup> To understand the role of pre-existing heterogeneities on the shock behavior of materials, we begin by examining inclusions, precipitates, and second-phase particles, as well as voids.

##### A. Inclusions: Second-phase particles, precipitates, and bubbles

The role of inclusions on shock and spall behavior, particularly spall strength, has been addressed for several multi-component systems via both experiments and simulations. Extensive work has been performed to understand the behavior of FCC materials under shock loading. As the field of shock developed, interest in alloys containing precipitates was apparent although the systematic nature needed to fully characterize the behavior was yet to be established. Murr and Foltz<sup>114</sup> investigated the shock deformation of Inconel 600 alloy to understand how precipitates of Cr and Fe altered the dynamic

behavior of Ni. Their experimental campaign aimed to understand if such inclusions would reduce dislocation mobility or act as additional dislocation sources; both dislocation sources and dislocation sinks were generated at particle–matrix interfaces and identified via TEM. Microstructural characterization shown in Fig. 6(a) exemplifies how microstructure had been historically characterized prior to shock loading. The sound speed and bulk composition were known, and the existing microstructure was characterized via grain size measurement and TEM imaging, neglecting precipitate composition, which limits the extent to which the role of microstructure can be evaluated.<sup>114</sup> Usually, simple measurements of density and sound speed are used to assess the effect of chemistry/composition on the dynamic response of materials. Results shown in Figs. 6(b) and 6(c), mainly consisting of TEM images, show profuse dislocations concentrated around the precipitates. Although specific composition, void growth, and velocimetry data were not reported, it is clear that precipitates played an important role in dislocation generation under shock loading.<sup>114</sup> A similar trend has been more detailed in direct numerical simulations, where Becker<sup>115</sup> and Callaghan<sup>116,117</sup> probed void growth localization due to precipitates in relation to strength modeling although this work is ongoing.

While the interest in the role of inclusions during shock loading has arisen throughout the literature, the systematic means of experimental study required to understand this phenomenon has been lacking until recently. Studies continue to focus on FCC materials, particularly Al and Cu. Becker and coworkers<sup>115–117</sup> investigated the effect of second phase particles and voids on tensile failure by spalling. They used finite element analysis which enabled them to capture the scale of microstructural inhomogeneities. Figure 7(a) shows a second-phase particle. A total of  $\sim 1000$  were generated. The matrix was modeled by J2 plasticity with a Steinberg constitutive equation incorporating both strain and strain-rate hardening. The second-phase particles have identical properties but have a low failure stress of 10 MPa which either causes their fracture or interfacial decohesion. A representative result [Fig. 7(b)] indicates that the failure path follows the existing particles. In addition to the spall plane, several particle

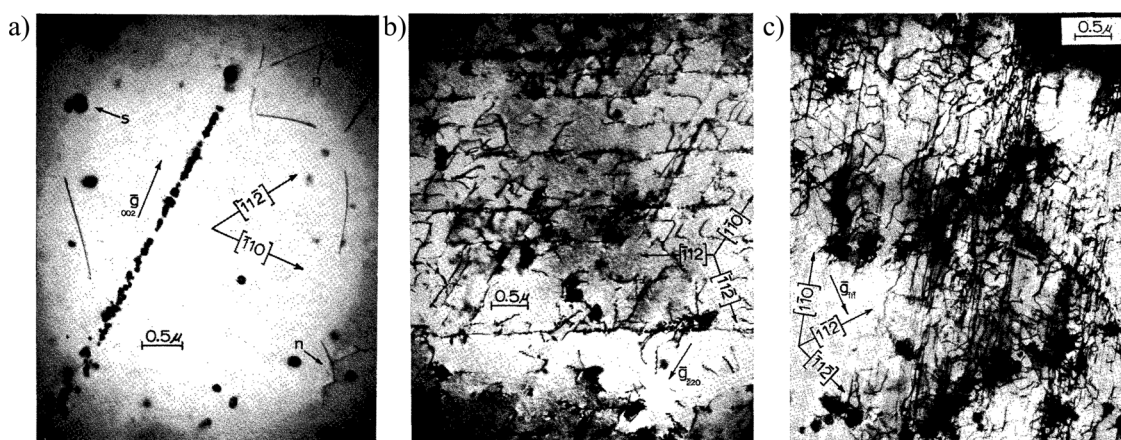


**FIG. 6.** (a) Unshocked Inconel microstructure showing precipitates and dislocations. (b) Residual microstructure of Inconel following 0.5 GPa shock. Dislocations appear concentrated around precipitates. (c) After 2.0 GPa shock loading, the precipitates remain intact with profuse networks of dislocations concentrated around them. Reproduced with permission from "Shock deformation of Inconel 600 alloy: Effect of fine coherent precipitates on explosive-shock hardening," *J. Appl. Phys.* **40**(9), 3796–3802 (1969). Copyright 1969 AIP Publishing.

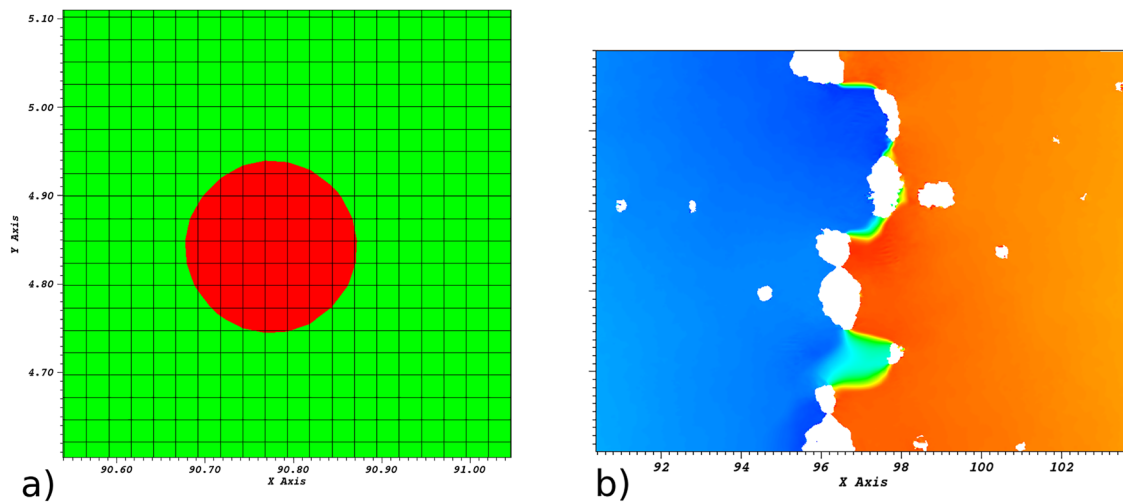


**FIG. 7.** (a) Representative particle with diameter of  $\sim 0.1 \mu\text{m}$  and (b) path of spall failure in matrix populated with particles with low tensile strength (10 MPa). Reproduced with permission from Becker and Callaghan, *Int. J. Fract.* **209**, 1 (2018). Copyright 2018 Elsevier.

sites can be seen that give rise to growing voids. Gas gun experiments by Gray<sup>118</sup> on a Cu matrix containing Nb precipitates at a peak shock pressure of 10 GPa demonstrated a decrease in shock hardening in comparison to Cu due to the differing compressive strain rate and temperature sensitivities between FCC Cu and BCC Nb, which likely results in an increase in defects stored in the Cu matrix. Further investigations by Hixson *et al.*<sup>23</sup> utilized gas gun experiments and simulations to elucidate the spall behavior of a Cu-Nb system. The inclusion morphology was well-documented, which allowed for the trends in free surface velocity to be linked to microstructure. The Cu/Nb system appeared indistinguishable from Oxygen Free Electric Grade (OFE) Cu, thus revealing the need for systematic experiments where samples were recovered and thoroughly characterized postmortem. To better understand the deformation mechanisms of Cu-Nb systems, Cu-Nb nanocomposites were studied via gas gun experiments where the initial material microstructure consisted of 135 nm thick layers alternating between Cu and Nb.<sup>119</sup> The composite material demonstrated a reduced spall strength compared to either single phase Cu or Nb, and spall failure was attributed to wave reflections at Cu-Nb interfaces which led to the nucleation, growth, and coalescence of voids within the Cu layers.

Fensin *et al.*<sup>13</sup> also examined the role of Nb (harder second phase, FCC/BCC interface) and Ag (softer second phase, FCC/FCC interface) using plate impact experiments. Cu + 24 wt. % Ag developed a eutectic microstructure, as shown in Fig. 8(a), whereas the Cu + 15 wt. % Nb formed elongated inclusions of Nb. The micrographs of post-spall recovered specimens are shown in Fig. 8(b). These micrographs were used to quantify the total damage during spall. The CuAg material displayed the largest void area, related to silver's preference for twinning (which generated nucleation sites), and an increased void growth in small-grained eutectic materials. The number of voids formed in CuAg in comparison to Cu was nearly twicw although their diameters were relatively similar. Conversely, CuNb nucleated the lowest number of voids although the void area of the CuNb material was similar to that of Cu; the Nb particles induced void growth in the local Cu matrix. Figures 8(c)–8(e) outline the changes in spall strength and

HEL for these materials. The CuAg material displayed a 6% increase in spall strength, possibly due to extensive twinning in Ag; the CuNb displayed a 26% increase in spall strength in comparison to polycrystalline Cu, likely due to Nb acting as a barrier to dislocation motion, inducing precipitation hardening. The significant differences in material microstructures likely altered the spall strength and the preferred nucleation and growth of damage in the material. This study emphasized the importance of different microstructures in controlling the dynamic behavior of metals. Specifically, this work showed that not all “bi-materials” behave in a similar way and that damage nucleation and growth may depend strongly upon the impedance mismatch between the constituent elements.<sup>15</sup>

MD simulations provide a crucial means of examining the *in situ* behavior of materials undergoing shock loading. MD simulations of nanocrystalline Cu embedded with Ta clusters (harder second phase, FCC/BCC interface) under shock loading revealed that FCC Ta clusters are more likely to form than BCC Ta clusters at radii less than 4.0 nm due to the FCC structure's lower formation energy; the presence of FCC Ta leads to a higher dislocation density in the nc-Cu/Ta system.<sup>120</sup> While Ta is a BCC material, probing the stability of an FCC phase was of interest due to the nanometer-scale cluster sizes required by MD simulations. Despite microstructural differences, the shock and spallation behavior are quite similar for both BCC and FCC Ta clusters although voids nucleated at the Cu-Ta interfaces during spall, illustrated in Figs. 9(a)–9(f). Pure nc-Cu overall had the highest dislocation density throughout shock loading while also having the highest spall strength; nc-Cu with BCC Ta clusters had the lowest spall strength. While grain size played a more significant role in spallation of the Cu/Ta, the number of Ta clusters and their size relative to the Cu grain size is the most dominant determinant for the spall strength in nc-Cu/Ta microstructures.<sup>120</sup> Similar to investigations of Cu-Nb, multilayered Cu/Ta microstructures have also been examined to isolate the role of the interfaces between the materials.<sup>121</sup> Flat interfaces generate deformation similar to single crystal Cu, enhance twinning in Cu layers, and demonstrate an increase in spall strength, whereas faceted interfaces, which more closely resemble inclusions, activate low

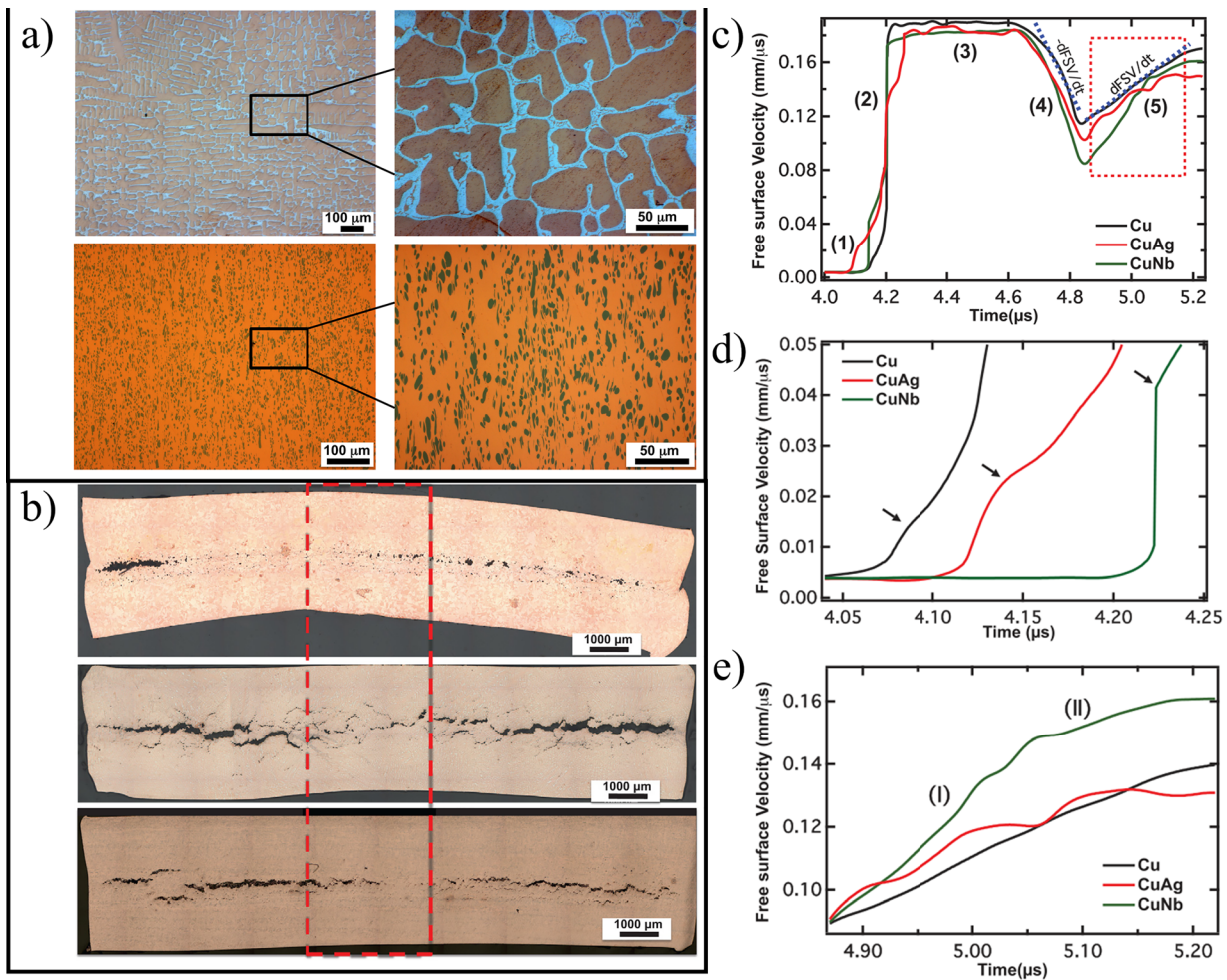


**FIG. 8.** (a) The initial microstructure of Cu-24%Ag (top) and Cu-15%Nb (bottom), where white regions in the top images show Ag and gray particles in the bottom images show Nb. (b) Micrographs of cross section of spalled Cu, CuAg, and CuNb, respectively, from top to bottom, with the spall plane located approximately central to each sample. The red box notes where analysis was performed to calculate void diameter via ImageJ. (c) The free surface velocity of the Cu, CuAg, and CuNb systems under shock loading. (d) The HEL is displayed in (d) while (e) depicts the free surface velocity rise following the minimum boxed in red in (c). Reproduced with permission from "Dynamic failure in two-phase materials," J. Appl. Phys. **118**(23), 235305 (2015). Copyright 2015 AIP Publishing.

Schmid factor secondary slip systems and lead to significant complex networks of twins throughout the multilayered microstructure. The lowest spall strengths correlate with interface-assisted heterogeneous dislocation nucleation for layer sizes less than 6 nm while larger interface spacing displays homogeneous dislocation nucleation.<sup>121</sup> Thus, the strength of a material can be weakened or strengthened depending on interface structure and spacing throughout.

As the properties of the precipitates change, they can alter the material overall response and their role in dictating the dynamic response of materials. Gas gun experiments performed on Cu and Cu + 1% Pb showed that the addition of a second softer phase decreased the spall strength of Cu by 45% due to the tendency of the Pb inclusions to nucleate voids.<sup>25</sup> This difference in spall behavior is clearly demonstrated in Figs. 10(a)–10(c), where each case has a distinct spall response. Specifically, while CuPb nucleated 80% more voids than pure Cu, these were found to be 50% smaller, implying

that the evolution of damage in CuPb is dominated by void nucleation, whereas it is dominated by void growth in pure Cu. The differences in damage between these cases are visually represented in Fig. 10(d). This work provides an important perspective on the role of second phase particles during shock, particularly on the required systematic nature of analysis directed at measuring damage, since several studies have examined the role of inclusions that are stronger than the surrounding matrix.<sup>25</sup> A recent study exploring the spall behavior of leaded brass (Cu-34Zn-3Pb) as a function of Pb inclusion size found a 5% reduction in spall strength when the area percentage of Pb inclusions is increased by 82%; note that the number of Pb inclusions is reduced for a greater area percentage.<sup>122</sup> Smaller Pb inclusions that occur more frequently serve as nucleation sites, thus increasing the damage rate, whereas larger, less frequent Pb inclusions serve as fewer nucleation sites that may facilitate higher damage growth rates. Interestingly, this study also finds that the

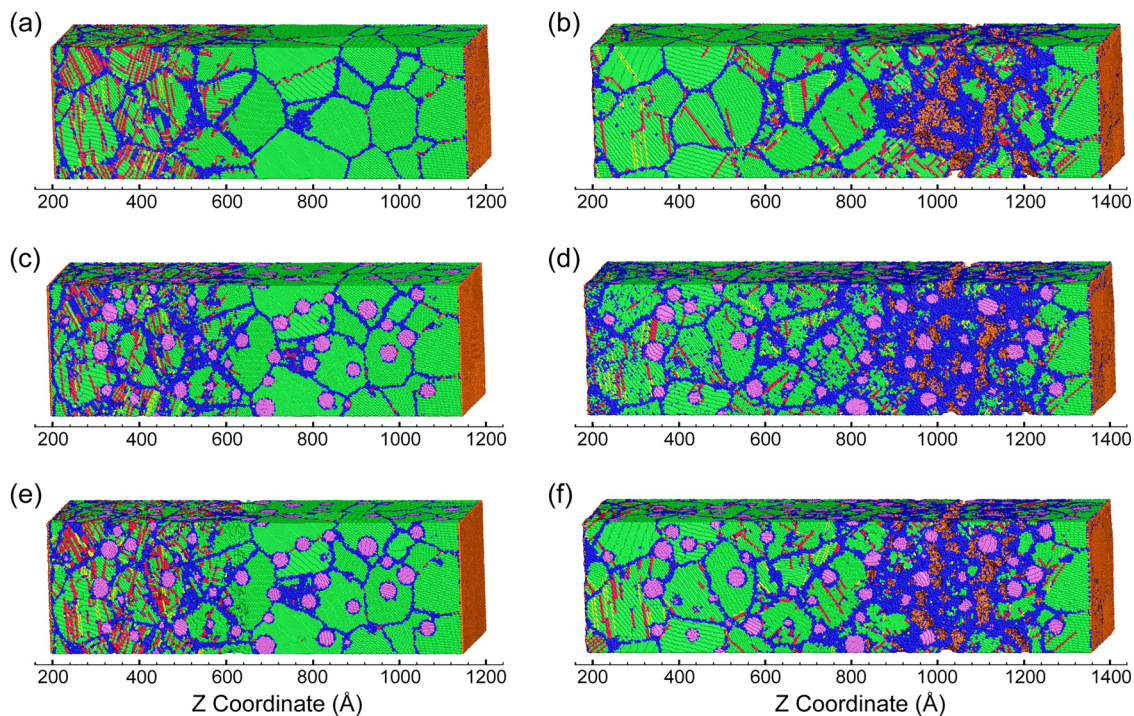


**FIG. 9.** [(a)–(e)] Deformation of nc-Cu/Ta systems at a particle velocity of 1.0 km/s. Atoms are colored green for Cu FCC stacking, red for stacking fault, yellow for twin faults, light blue for twinning partials, blue for disordered atoms, purple for Ta atoms, and orange for a surface. Left images [(a), (c), and (e)] are taken at 10 ps while right images [(b), (d), and (f)] are taken at peak tensile stress at 30 ps. [(a) and (b)] Pure nc-Cu. [(c) and (d)] FCC Ta clusters and [(e) and (f)] BCC Ta clusters. An overall concentration of 6.3% of Ta and an average grain diameter of 3.0 nm. (g) Spall strength of nc-Cu/Ta systems as a function of Ta concentration. Reproduced with permission from Chen *et al.*, *J. Mater. Sci.* **53**, 8 (2018). Copyright 2018 Springer.

voids nucleate within the Pb inclusions, possibly due to the localized reflection of shock waves at phase boundaries, but further experiments are necessary.<sup>122</sup>

Copper matrices have been of particular interest due to the well-documented behavior of pure copper, but a myriad of more complex alloys with various microstructures have also been characterized under shock loading although the emphasis has been on grain size and shock-loading parameters such as thickness, impact stress, and strain rate. Even when impurities are included, they are mentioned quite briefly. For example, Chen *et al.*<sup>26</sup> investigated multiple alloys of Al including variation of texture of the overall microstructure; they mainly focused on grain size effects, but briefly mentioned that at 22 GPa, a 6061-80 alloy with “both fine and coarse impurities” has a spall strength comparable to the [111] single crystal, thus suggesting that microstructure is perhaps not as important at increased impact stresses. The challenge in understanding the role of such inclusions is systematic characterization of the microstructure itself prior to experiments, which can then be related to trends in that data postmortem. Huang and Gray<sup>123</sup> explored the mechanical response of two Al-Li-Cu alloys via shock loading. Split Hopkinson Pressure Bar (SHPB) compression, and quasistatic compression in order to examine the defect substructure evolution. Precipitates of  $\text{Al}_3\text{Li}$  and  $\text{Al}_3\text{Zr}$  were embedded in Al-Li-Cu alloys via different aging processes, yielding a variety of volume fractions and precipitate diameters in each material. In comparison to studies of shock-loaded pure Al, significantly more localized

band deformation and dislocation loops were observed in this study. While most alloys demonstrated a band-like deformation structure, the overaged Li-rich alloy lacked this band structure and planar localization, instead exhibiting an increase in dislocation loops, which were thought to have nucleated from precipitates. While this study did not quantify the change in dynamic behavior due to the precipitates, the authors again identified precipitates as playing an important role in material deformation.<sup>123</sup>

Varying methods for processing alloys can alter the microstructure of a material significantly enough to affect its behavior under shock loading due to changes in the grain boundary structure, formation of precipitates, or addition of impurities. In the case of 5083 Al, equal-channel angular extrusion (ECAE) processing was shown to noticeably alter the spall strength of the material. Rolled 5083-H321 Al was processed via ECAE and then cold-rolled to a 30% reduction in thickness; second phase intermetallic clusters were present throughout the as-received material, and the ECAE and cold-rolling treatment resulted in smaller clusters.<sup>124</sup> The treated material displayed an  $\sim 78\%$  increase in HEL, but a 23%–37% decrease in spall strength in comparison to the 5083-H321 as-received alloy. Although debonding of Mn-Fe rich particles was observed during shock compression, failure along the realigned particles appeared to be the main source of spall failure for the cold-rolled material, while the 5083-H321 as-received aluminum displayed mixed-mode failure due to complex void nucleation.<sup>124</sup> While cold-rolling increased the HEL of the

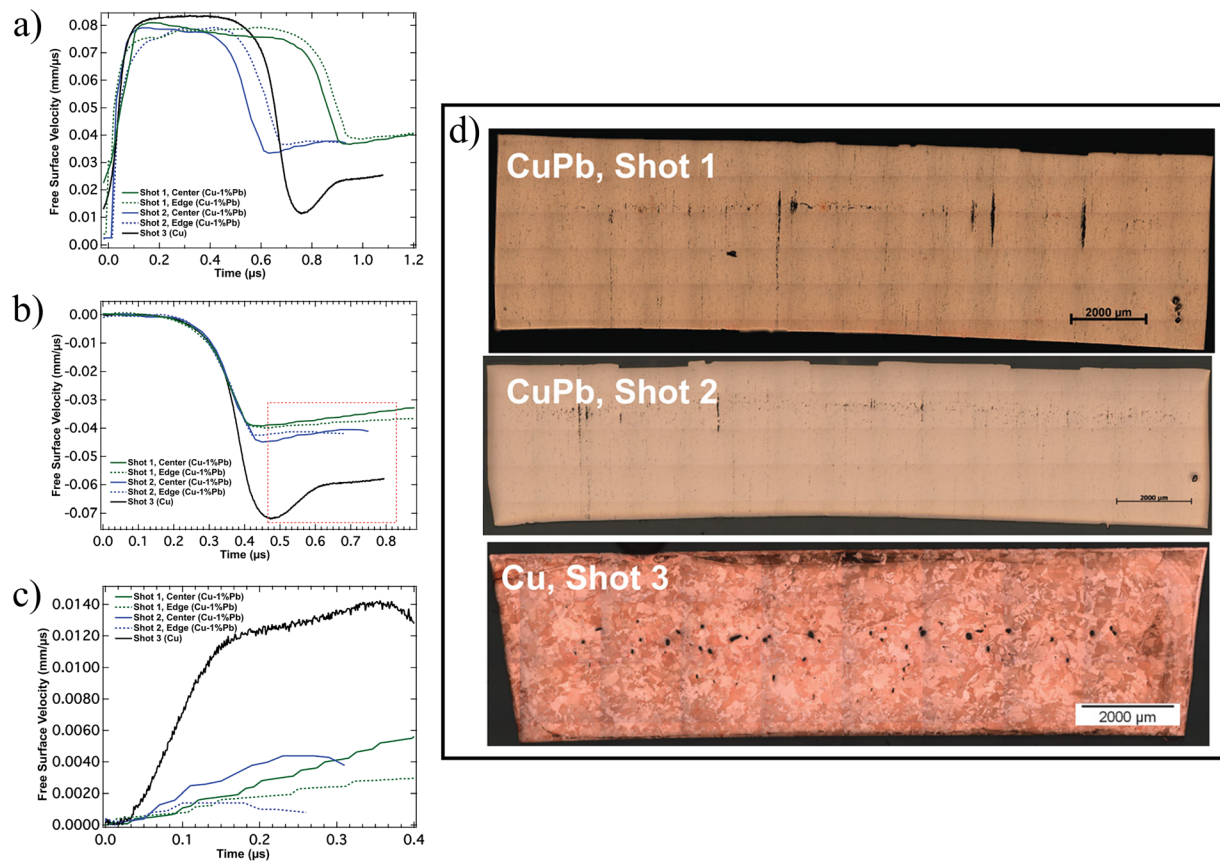


**FIG. 10.** (a) Free surface velocity of shock loading experiments on Cu and CuPb, with solid and dotted lines corresponding to probes placed on the center and edge of the samples, respectively. (b) Region of (a) associated with the pullback velocity, characteristic of spallation. (c) Free surface velocity after the minimum. (d) Optical micrographs of recovered samples, where the spall plane lies approximately in the middle of the sample and the large black spots represent voids. Note that smaller black Pb particles and voids both appear black. Reproduced with permission from "Dynamic damage nucleation and evolution in multiphase materials," *J. Appl. Phys.* **115**(20), 203516 (2014). Copyright 2014 AIP Publishing.

material, the precipitates served as nucleation sites for damage, leading to a decrease in spall strength for the ECAE and cold-rolled material.

The relationship between processing and microstructure is also prevalent among studies of Mg alloys. Spall experiments via gas gun were performed to measure the dynamic properties of the AZ31B-4E Mg, a Mg alloy treated via ECAE.<sup>125</sup> Significant amounts of heterogeneous and irregularly shaped secondary phases spaced 65 μm apart were found in the unshocked material. Scanning electron microscopy (SEM) micrographs shown in Figs. 11(a)–11(c) illustrate this microstructure. These second-phase inclusions are predicted to impede dislocation motion, thereby increasing the spall strength. Energy-dispersive x-ray spectroscopy (EDS) analysis suggested that the large phases were intermetallic and composed of Al, Mn, and Fe, while the smaller precipitates were comprised of Al and Zn, as shown in Figs. 11(d)–11(i). Results of the spall strength measurements and spall recovery experiments are summarized in Fig. 12. It was proposed that the ECAE treatment increased the spall strength, but Fig. 12(a) in comparison to previous results<sup>126</sup> shows that ECAE led to a 5% weakening of the material; further testing is required since the difference is

fairly low. Figure 12(b) shows multiple spall planes within the material. Localization of voids was identified within the neighboring matrix of the inclusions as well as the development of microvoids at the inclusion–matrix interface, detailed in Figs. 12(c)–12(e). The intermetallic particles embedded in the material were responsible for the initiation of spall in this alloy, thus weakening the material similar to results discussed above.<sup>125</sup>

To follow up the aforementioned results on AZ31B, Kryowpusk *et al.*<sup>127</sup> performed spall recovery experiments to better understand the role played by large Mn-Al particles formed during material processing. For samples impacted at 200 m/s, the majority of incipient voids formed from fractured Mn-Al particles and grew via brittle crack propagation within the particles, but there were incipient voids which formed in the matrix with an equiaxed structure. Samples shocked at 400 m/s demonstrated far more spall damage, with localized nano-voids formed within Al-Zn precipitates as observed by Farbaniec *et al.*<sup>125</sup> Using fractography and EBSD, Kryowpusk *et al.*<sup>127</sup> confirmed that the Mn-Al particles were an initial source of voids, which underwent an internal brittle fracture before nucleating more ductile

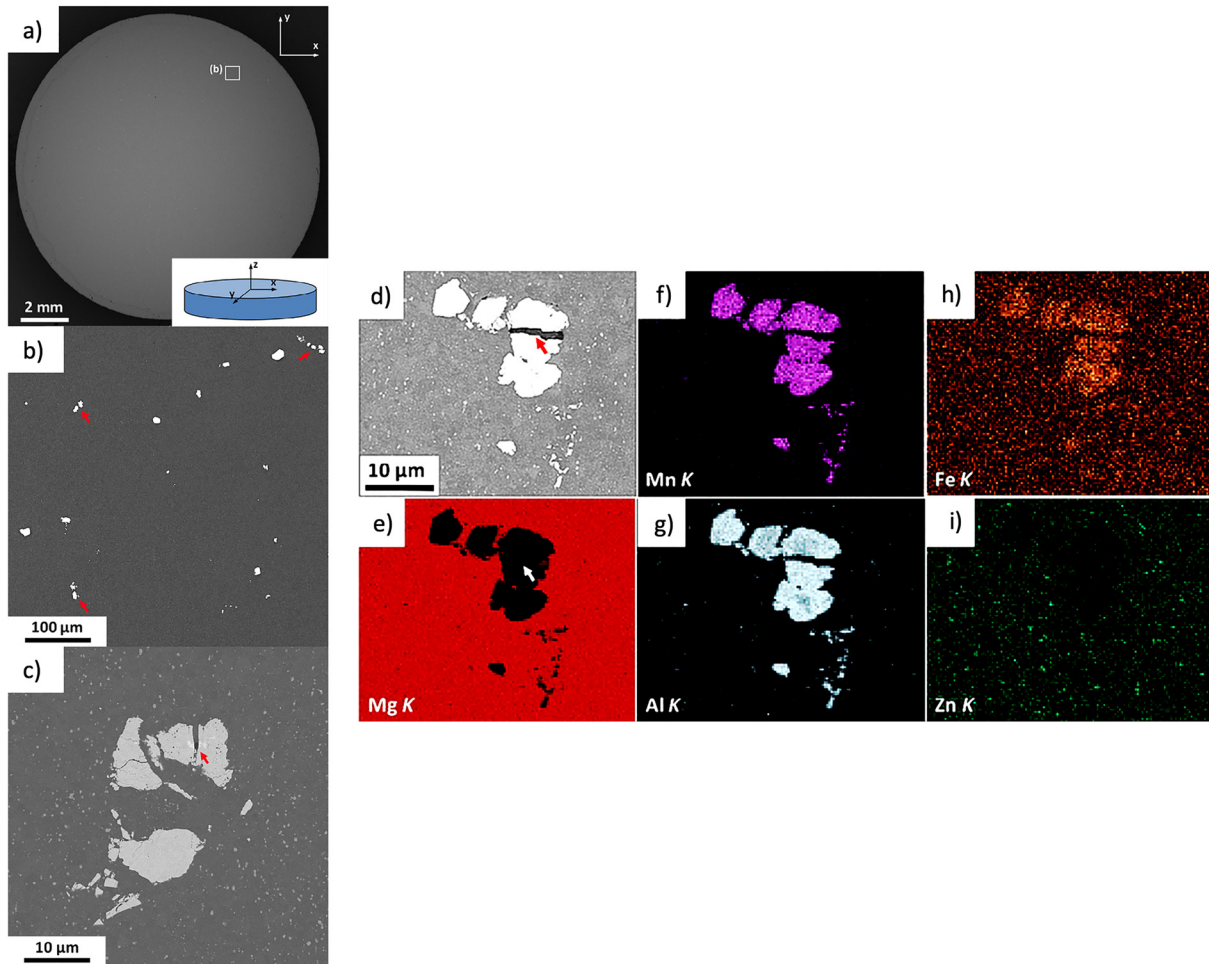


**FIG. 11.** Pre-shock microstructural characterization of AZ31B-4E Mg alloy. [(a)–(c)] Backscattered electron contrast micrographs of AZ31B-4E Mg alloy prior to shock loading. (a) Entire specimen. (b) Zoomed-in surface showing secondary phases. (c) Highest magnification showing one cluster of secondary phases and precipitates present in the initial microstructure. [(d)–(i)] Combined SEM/EDS map showing (d) SEM micrograph of the defect of interest. [(e) and (b)] Mg shown via EDS elemental map. (f) Mn shown via EDS elemental map. (g) Al shown via EDS elemental map. (h) Fe shown via EDS elemental map. (i) Zn shown via EDS elemental map. Reproduced with permission from Farbaniec *et al.*, *Int. J. Impact Eng.* **98**, 34–41 (2016). Copyright 2016 Elsevier.

cracking in the matrix. Twinning was predicted to play a role in the formation of inter-void cracks between the Mn-Al particles. This work demonstrates the importance of microstructure beyond grain size, particularly because a study which set out to understand the texture dependence of the alloy actually emphasizes the role of the Mn-Al particles in dictating failure in materials.<sup>127</sup>

While the majority of studies have focused on intermetallic structures, understandably due to the prevalence of such materials in practical engineering application, nonmetal inclusions have been probed as well. Using gas gun experiments, Hixson *et al.*<sup>23</sup> sought to elucidate the role of alumina in the spall behavior of pure Al. The Al-Al<sub>2</sub>O<sub>3</sub> composites showed a clear decrease in spall strength in comparison with bulk Al by up to 60%. Although one may assume this is due to weak interfacial bonds, the authors note that they believe this bond to be fairly strong and postulate that the difference in elastic moduli between the ceramic inclusion and the Al matrix leads to substantial

hydrostatic tension, causing voids to nucleate and grow close to the interface.<sup>23</sup> A similar study by Razorenov *et al.*<sup>24</sup> examined the role of 0.1% Si and SiO<sub>2</sub> inclusions in the dynamic response of polycrystalline Cu using explosives and gas gun experiments. The 0.1% Si formed a solid solution with Cu while SiO<sub>2</sub> formed particles of average size of 0.18 μm separated by 0.5–5 μm within the Cu matrix. Figure 13(a) shows the measured spall strength for all cases considered in this work, revealing that Cu with 0.1% Si had lower spall strength than pure Cu, followed by Cu with SiO<sub>2</sub> and polycrystalline Cu. The spall surfaces in both Cu + 0.1% Si and Cu + SiO<sub>2</sub> are compared in Figs. 13(b) and 13(c). Ductile failure is observed in both with the ductile dimple size of ~2-μm in SiO<sub>2</sub>, which also coincides with spacing between the SiO<sub>2</sub> particles, suggesting that the silica served as a nucleation site. Meanwhile, the size of the ductile dimples was ~4 and 40 μm in Cu with 0.1% Si. The difference in the size of the ductile dimples was used to conclude that while failure was dominated by void

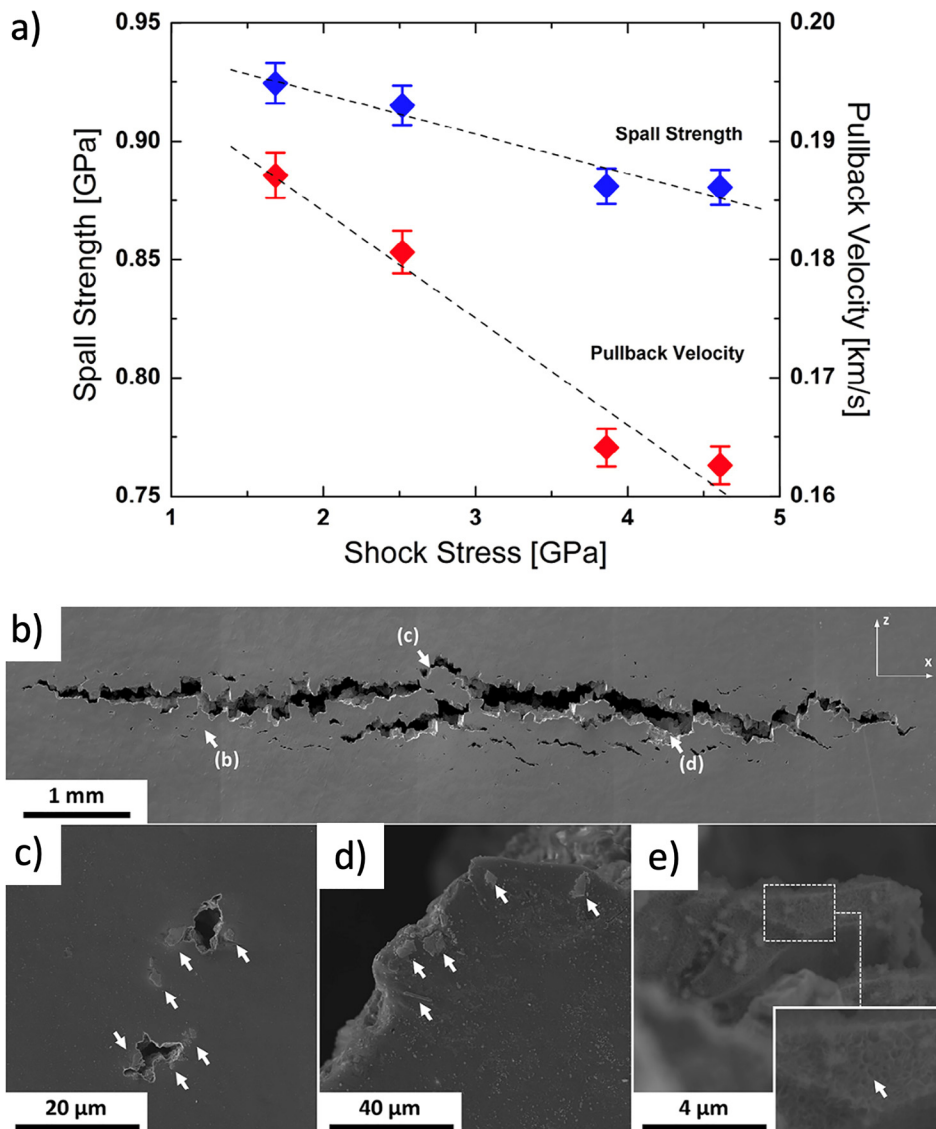


**FIG. 12.** (a) Spall strength and pullback velocity as a function of shock stress for AZ31B-4E Mg alloy. (b) SEM of a recovered specimen at 401 m/s, showing a damage zone with multiple spall planes. (c) Void growth and coalescence originating from clustered inclusions indicated by arrows. (d) Inclusions at the edge of spall plane. (e) Inclusions found within the spall plane. Reproduced with permission from Farbaniec *et al.*, *Int. J. Impact Eng.* **98**, 34–41 (2016). Copyright 2016 Elsevier.

nucleation in Cu with SiO<sub>2</sub>, it was growth dominated in Cu with 0.1% Si. Further, the silicon particles were assumed to be randomly distributed throughout the Cu with 0.1% Si, which caused a heterogeneous nucleation of damage concentrated at grain boundaries.<sup>24</sup> Additional work by Minich *et al.*<sup>20</sup> on Cu with SiO<sub>2</sub> reported the orientation dependence of the spall strength in Cu. This work showed that single crystal Cu embedded with silica (SiO<sub>2</sub>), whose initial microstructure is shown in Fig. 14(a), displayed a distinct decrease in pullback velocity as shock pressure increased in comparison to polycrystalline and single crystal Cu as shown in Fig. 14(b).<sup>20</sup> The work by Minich *et al.*,<sup>20</sup> as previously mentioned, probes the anisotropic nature of Cu under shock loading as well as the role of grain size; while each of these microstructural conditions has a marked effect on the spall strength of Cu, the addition of silica results in a significantly smaller

spall strength despite being embedded in a single crystal that otherwise was recorded to have the greatest spall strength throughout the study. This may be due to the silica particle's increased capacity for nucleating damage since the inclusions are small and much harder than the Cu matrix. The data clearly showed that addition of SiO<sub>2</sub> to Cu caused an obvious change in strength, as was shown in the study by Razorenov *et al.*,<sup>24</sup> but the work by Minich *et al.*<sup>20</sup> also indicates that the interplay between precipitates and grain boundaries must also be explored in order to ascertain and characterize the dominant phenomenon.

While ceramic inclusions have been probed in Cu matrices, boron embedded in Al exemplifies another case of nonmetallic inclusions. The impact of second phase particles of boron with concentration of 0.07 and 0.15 wt. % in Al was explored via gas gun experiments,

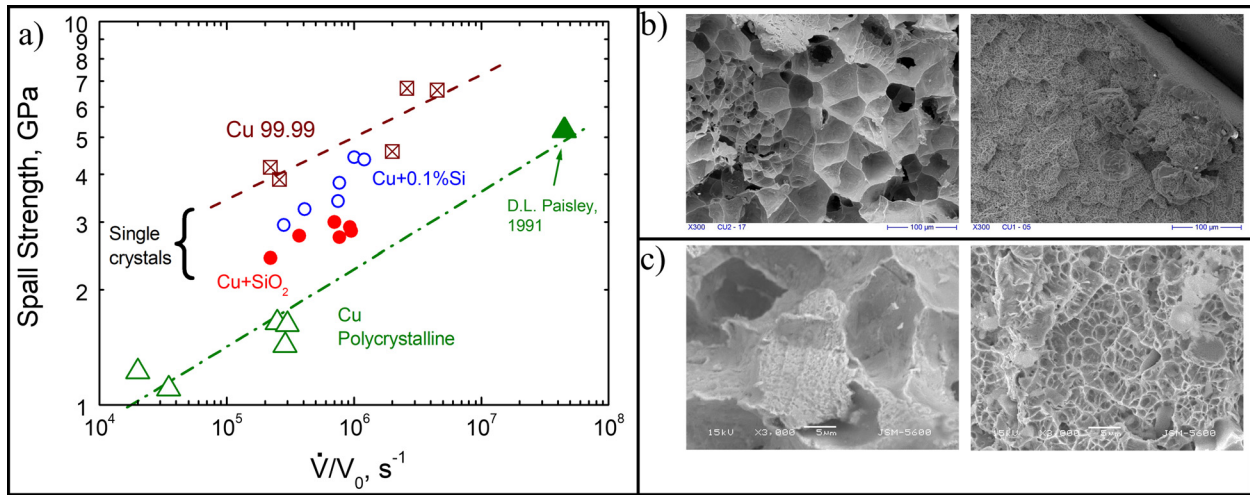


FIG. 13. (a) Spall strength as a function of rarefaction rate for Cu, Cu + SiO<sub>2</sub>, and Cu + 0.1% Si from Ref. 24. (b) SEM images comparing the spall plane for Cu + 0.1% (left) and Cu + SiO<sub>2</sub> (right). (c) High-resolution SEM images of the spall surface for Cu + 0.1% (left) and Cu + SiO<sub>2</sub> (right). Reproduced with permission from "Influence of nano-size inclusions on spall fracture of copper single crystals," AIP Conf. Proc. 955(1), 581–584 (2007). Copyright 2007 AIP Publishing.

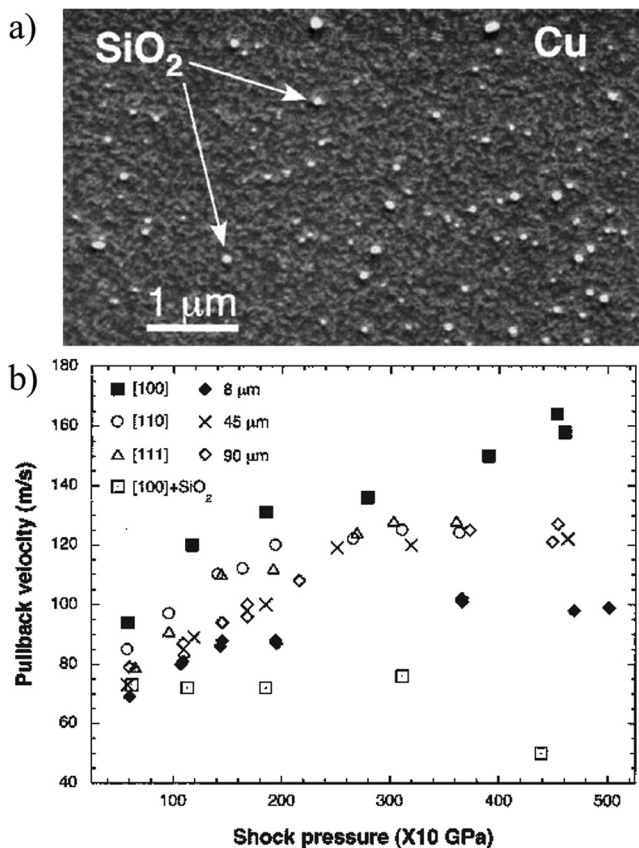
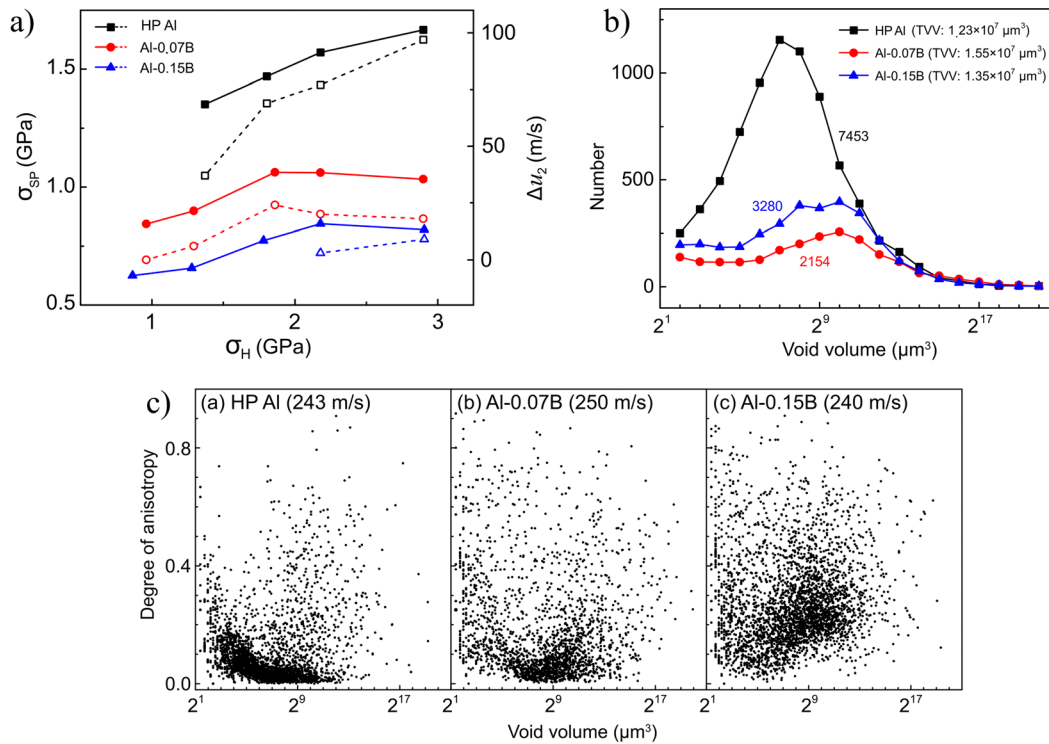


FIG. 14. (a) SEM image of Cu + SiO<sub>2</sub> from Ref. 20 showing nearly uniform distribution of SiO<sub>2</sub> throughout a single crystal copper matrix. (b) Summary of the spall strength as a function of shock pressure for various copper microstructures. Reproduced with permission from Minich *et al.*, Metall. Mater. Trans. A 35, 9 (2004). Copyright 2004 Springer.

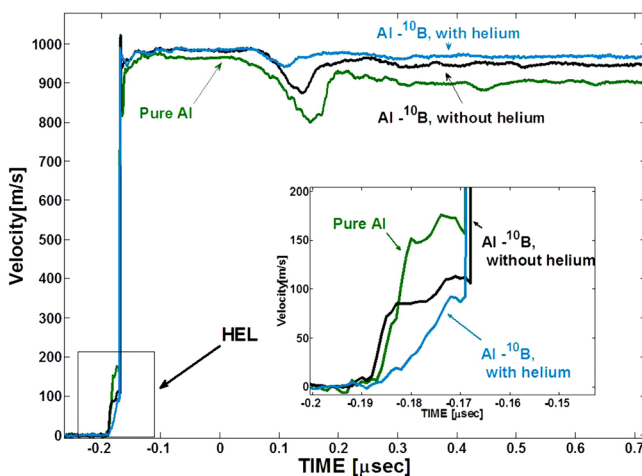
revealing that an increase in boron concentration corresponded to a decrease in spall strength by 30%, shown in Fig. 15(a), although there was a negligible change in the HEL.<sup>27</sup> Second-phase weakening was observed in the increased spread of damage away from the spall plane, and the boron inclusions led to increased anisotropy and damage, thus reducing the spall strength. The quantification of the void volume is important because it shows that there were fewer voids as the concentration of the precipitates decreased, shown in Fig. 15(b). The reduced number of voids coupled with the reduction in spall strength implies that void coalescence is the primary means by which failure occurs in materials with boron precipitates. The measure of void anisotropy is shown in Fig. 15(c). Voids with an equiaxed, spherical structure have a degree of anisotropy of 0, while a degree of anisotropy of 1 is achieved when the ratio of long axis to short axis is infinite. High purity Al and Al-0.07B have fairly low anisotropy in their void geometry, suggesting that void growth is the dominant means of failure. For Al-0.15B, the degree of anisotropy has the greatest variation, especially for large voids, reinforcing the dominance of void coalescence during spallation. This is attributed to the increase in particle–matrix interfaces, which increases as the boron concentration increases.<sup>27</sup>

Understanding the role of B inclusions in Al is extended to the case where He impurities are also present in materials.<sup>128,129</sup> Shock compression experiments via gas gun of Al revealed a marked decrease in the HEL of the material when implanted with boron and helium impurities throughout the thickness of the samples. At 600 °C, the HEL was substantially higher for all targets due the dominance of phonon drag, but the HEL for the helium implanted case was indistinguishable from pure Al.<sup>128,129</sup> Figure 16 outlines the results for these experiments, showing the change in HEL as well as the differences in pullback velocity. Although processed in a similar manner, the change in HEL between pure Al and Al-B without helium bubbles may be attributed to the differences in grain size, aligning with the Hall–Petch equation discussed earlier.<sup>71,72</sup> At room temperature, the Al-B and Al-B-He experiments yielded nearly the same spall strength, but at 600 °C preheating, the helium-implanted material displayed a substantially



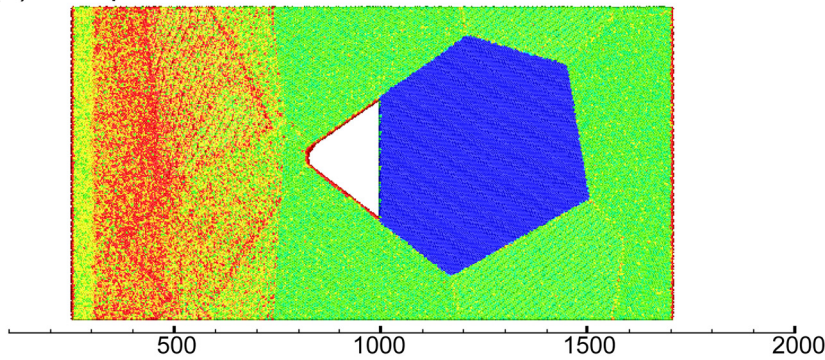
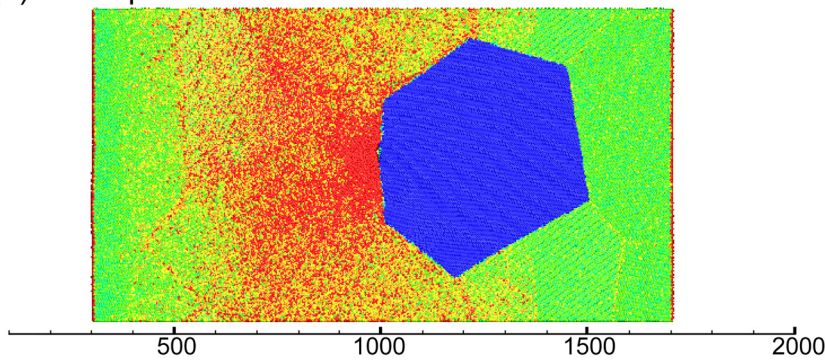
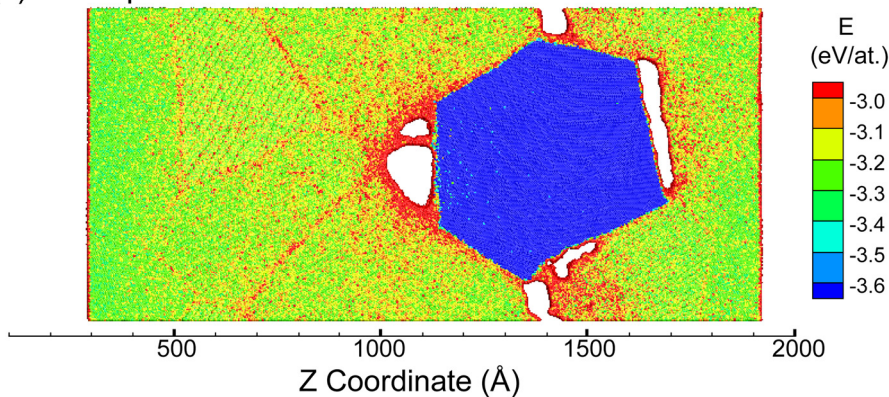
**FIG. 15.** (a) Pullback velocity (dashed lines) and spall strength (solid lines) for high purity Al, Al + 0.07% B, and Al + 0.15% B as a function of peak stress. (b) Number of voids vs void volume, noting the total number of voids. Note that TVV stands for total volume of voids. (c) Anisotropy measured via void shape as a function of void volume for samples at similar impact velocities. Reproduced with permission from Cheng *et al.*, Mater. Sci. Eng. A **793**, 139805 (2020). Copyright 2020 Elsevier.

smaller decrease in spall strength compared to pure Al and Al-B, likely due to the role played by He bubbles in the spallation process. More work is required to characterize recovered material and the damage present therein.<sup>128,129</sup>



**FIG. 16.** Free surface velocity for gas gun experiments of Al, Al-B, and Al-B-He systems. The HEL is shown in the inset. Reproduced with permission from Glam *et al.*, Int. J. Impact Eng. **65**, 1–12 (2014). Copyright 2014 Elsevier.

Dongare<sup>130,131</sup> used molecular dynamics to understand damage nucleation and evolution under shock in the presence of interfaces and in a composed microstructure as shown in Fig. 17(a). This figure shows a nickel grain (blue) embedded in an aluminum matrix (green), along with a triangular void (white) and captures the presence of both the porosity and interfaces in an initial microstructure. The shock compression wave travels from left to right; upon collapse of the void [Fig. 17(b)], there is a clear increase in the temperature, indicated by the red color in energy. The scale represents energy units of eV/atom. The highest value is  $-3eV/atom$ , whereas the lowest value is  $-3.6eV/atom$ . The snapshot in Fig. 17(b) illustrates the temperature rise, which reaches 1000 K at 14 ps. When the compression wave reflects, generating tension, failure occurs preferentially at the interface of the nickel particle [Fig. 17(c)]. In order to expand the spatial and temporal capability of MD, mostly hundreds of nanometers and picosecond, Dongare<sup>130,131</sup> applied a coarse-grained model, using sets of atoms rather than individual atoms in MD. He named this “quasi-coarse-grained dynamics” (QCGD). Coarse graining is a well-known strata-gem used to extend the capability of MD. The blocks of atoms are subjected to appropriate potentials which provide equivalent energy levels and can handle larger microstructures which more closely resemble real ones. Figure 18 shows layers of monocrystalline copper separated by interfaces (blue) and subjected to tension. The defects, in red, are stacking faults and dislocations. Both MD and QCGD are shown. These results show that the quasi-coarse grained approach produces

(a)  $t = 6$  ps(b)  $t = 14$  ps(c)  $t = 40$  ps

**FIG. 17.** MD simulation of shock wave propagating into aluminum containing a nickel particle (blue) and void (white); (a) shock wave in aluminum with inhomogeneous temperature rise due to defects; (b) collapse of voids at 14 ps; (c) release wave generating decohesion and plastic void growth surrounding nickel particle. Reproduced with permission from Dongare, *Philos. Mag.* **94**, 34 (2014). Copyright 2014 Taylor and Francis.

an evolution of defects similar to MD. Thus, QCGD may allow for better comparisons between simulations and experiments.<sup>130,131</sup>

Based on the studies outlined above, precipitates, second phase particles, and inclusions alter the shock behavior of the material by serving as dislocation sources and nucleation sites for voids, creating localized failure within the material rather than strengthening it as previous hypotheses had predicted under uniaxial stress loading. Also, the specific role played by these second phases is dependent not only on their role in deformation during shock compression but also on the impedance mismatch between them and the material matrix.

## B. Voids

Considerable research has been conducted to understand how pre-existing voids behave under shock loading, especially due to substantial interest in porous and explosive media, where voids can generate hot spots and initiate detonation.<sup>132–137</sup> Early simulations on the role of pre-existing voids focused on extremely simple cases such as 2D voids, cylindrical voids, and void-induced detonation<sup>134–137</sup> with early models suggesting that voids emit prismatic dislocation loops during collapse.<sup>138,139</sup> However, later simulations show that dislocation

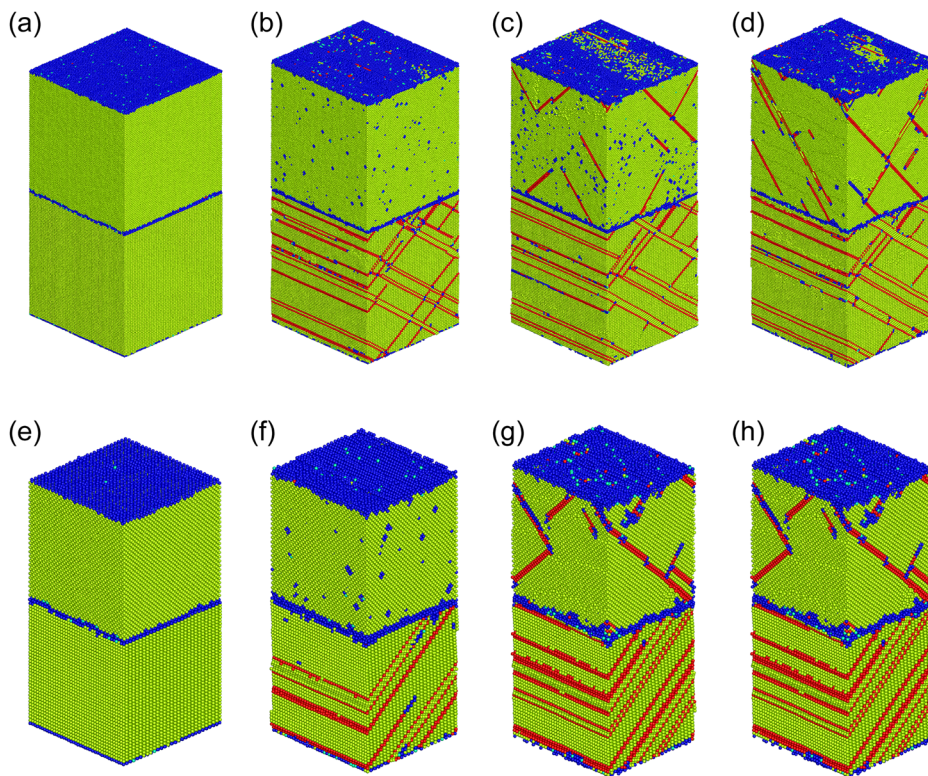


**FIG. 18.** Microstructure consisting of layer of copper atoms (green) separated by blue interfaces. [(a)–(d)] MD simulations; [(e)–(h)] coarse graining (QCGD). The applied tensile strains increase from left to right and the corresponding density of generated defects (dislocations and stacking faults) increases correspondingly. Reproduced with permission from Dongare, *J. Mater. Sci.* **55**(8), 3157–3166 (2020). Copyright 2020 Springer.

loops emitted during void collapse are shear loops, thus generating intense plastic deformation adjacent to the collapsing voids.<sup>140–142</sup> The development of shear loops has been linked to geometrically necessary dislocations (GNDs), demonstrating that as a cavity collapses, shear dislocation loops carry matter away from the void, thus coupling the processes of compaction and plasticity.<sup>143</sup> Much of the work performed to understand the role of pre-existing voids in metals has been done via simulations rather than experiments due to experimental challenges with temporal and spatial resolution. It is important to note that a significant interest in hot spot formation due to the presence of voids in materials developed in order to better understand explosive materials, but for the sake of simplicity, we opt to focus on nonreactive materials.

Bourne<sup>144</sup> performed extensive work on the collapse of pre-existing voids under shock loading for a variety of materials, exemplified by the cavity collapse images shown in Fig. 19. Bourne's 2002 review<sup>144</sup> summarizes the collapse of cavities, outlining the mechanical effects of collapse and past efforts to understand the response of cavities under dynamic loading, concluding that more complete descriptions require accurate and time-resolved measurements. Despite assumptions of symmetry and spherical collapse, adjacent bubbles and boundaries combined with acceleration of a cavity's upstream wall under shock loading, followed by impact of a jet during collapse, complicate the problem of interest. Many studies have emphasized the collapse of single cavities although a single isolated cavity is rare. Collapse time of the cavity plays a role in the temperature increase, and the velocity of an internal liquid jet increases as the cavity diameter is decreased. Although more work such as accurate, time-resolved measurements of

temperature and an understanding the complex interactions within a field of cavities is necessary, Bourne<sup>144</sup> concluded that cavity collapse is an integrated function of parameters such as the materials and the conditions to which they are subjected.

MD simulations became a prevalent means for understanding nanoscale behavior, particularly for materials under shock loading, due to the short timescale during which shock occurs. MD simulations numerically solve Newton's second law for individual atoms within a material using a force-field potential function, which is parameterized based on measured interactions between atoms on the quantum scale. Using a Lennard-Jones potential (the most basic two-body potential function), Phillips *et al.*<sup>137</sup> sought to understand hot spot formation under shock loading by implanting two-dimensional perfect crystals with voids and bubbles of various sizes and shocking them at a velocity of 4.258 km/s. Phillips *et al.*<sup>137</sup> found that defect collapse leads to a localization of a fluid-like phase with increased temperature and density, however, noting that further simulations and experiments are necessary to more accurately illustrate their observations.

A subsequent study by Holian *et al.*<sup>134</sup> suggested that hot spot generation required a shock sufficiently strong to eject atoms into a pre-existing void and the collision of ejected particles with the far side of the void. Unsatisfied with the quantitative results and the local behavior involved with hot spot formation, Hatano<sup>132,133</sup> responded by examining the dynamic aspect of shock-induced chemistry during void collapse, which he noted to be a strongly nonequilibrium phenomenon. Using MD simulations, Hatano<sup>132,133</sup> found that the maximum temperature and velocity are realized at the beginning of

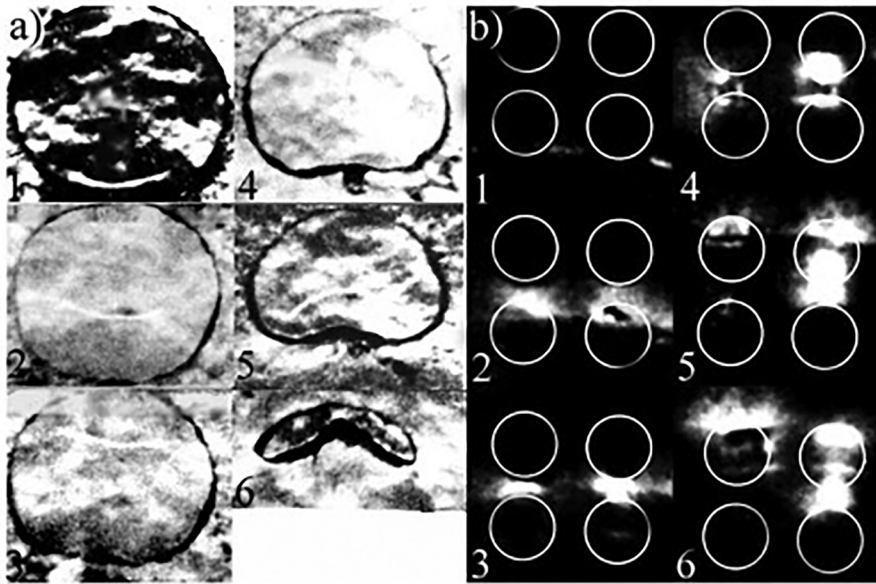


**FIG. 19.** (a) A 12 mm cavity in gelatin collapses starting at  $5 \mu\text{s}$  in frame 1 from the time that the shock arrives at the cavity. Frame 2 is taken at  $15 \mu\text{s}$ , frame 3 at  $25 \mu\text{s}$ , 4 at  $45 \mu\text{s}$ , 5 at  $65 \mu\text{s}$ , and 6 at  $105 \mu\text{s}$ . (b) A series of four 5 mm cavities subjected to shock compression of 8 GPa. The white ring indicates the initial location of the cavity. Each frame was taken  $1 \mu\text{s}$  apart. Reproduced with permission from Bourne, *Shock Waves* 11(6), 447–455 (2002). Copyright 2002 Springer.

collapse, whereas energetic intermolecular collisions are maximized when the void has finished collapsing. A large cross-sectional area correlates with an increase in collisions while transverse length relates to a change in temperature. Even with a simplified Lennard-Jones potential, Hatano<sup>133</sup> demonstrated the nucleation of partial dislocation loops from the surface of a void and the subsequent development of sessile dislocations. Work by Hatano<sup>132,133</sup> elucidated important aspects of the role played by pre-existing defects in the shock response although computational restrictions limit the applicability to large metallic systems.

MD simulations of Cu containing pre-existing voids with radii of 1.5 and 2 nm subjected to shock loading were performed by Davila *et al.*<sup>140</sup> While previous studies performed via MD simulations suggested that prismatic dislocation loops were the mechanism by which voids collapsed, Davila *et al.* showed that this is achieved via shear dislocation loops. Figure 20(a) demonstrates the step-by-step emission of dislocation loops from a void with radius of 1.5 nm shocked to 8 GPa. As the void collapses, shear dislocation loops are emitted. Figure 20(b) displays the stress for emission of dislocations as a function of void radius, comparing earlier work<sup>139</sup> to that of Huang and Gray.<sup>123</sup> Using a model by Lubarda *et al.*<sup>145</sup> to predict the stress required for dislocation generation via void growth, Davila *et al.*<sup>140</sup> showed that the generation of shear loops via void collapse followed a similar trend.

He *et al.*<sup>146</sup> also performed MD simulations of Cu containing pre-existing voids of radius 2.0 nm along the [001] direction using piston velocities from 2.75–3.3 km/s. This study aimed to explore the interplay between pre-existing voids and shock-induced melting. Figure 21(a) shows that the nanovoid did not significantly alter the melting point of the bulk material, but a small decline in global order is shown in Fig. 21(b), possibly due to localized, heterogeneous shock melting. Figures 21(c)–21(f) show the localized behavior of the void 0.5 ps after the shock front has passed; the observed disorder confirmed that heterogeneous local melting in the collapsed void region does occur. Similar work via MD simulations on [111] Cu demonstrated localized shock melting adjacent to voids and He bubbles, and

suggests that the shock front becomes nonplanar in that region due to the collapse of voids and localized melting.<sup>147</sup> He *et al.*<sup>146</sup> found that, as the region cools, the liquid phase will recrystallize, or at higher shock strengths, remain liquid, and grow throughout the material; they identify a decrease in superheating for the void collapsed region (7%) in comparison to the perfect crystal (14%).

A thorough study of growth and collapse of voids in Ta was performed via MD simulations to understand the multitude of deformation mechanisms as stress state and strain rate are changed.<sup>148</sup> For the sake of simplicity, we focus on the compressive strain case since it is most directly relevant to achieving the goal of this review. Pre-existing voids with a radius of 3.3 nm were generated in Ta and subjected to  $\sim 15$  GPa shock compression. The generation of shear loops from the surface of the void is shown in Fig. 22(a) for strain rates of  $10^8$  (left) and  $10^{10} \text{ s}^{-1}$  (right). Twinning is not observed with a change in strain rate, likely due to the formation of screw dislocations under compression, which prefer to glide in {110} planes regardless of strain rate. Interestingly, laser shock experiments at a strain rate of  $10^9 \text{ s}^{-1}$  on Ta demonstrated deformation via dislocation glide at 15 GPa but twinning under stresses exceeding 35 GPa; this is demonstrated in Fig. 22(b). Note that these experiments did not characterize any pre-existing microstructure. While this study examined the role of pre-existing voids under shock via simulations, it also demonstrated the challenges in experimental shock studies and the importance of characterizing microstructure prior to shock loading.<sup>148</sup> Collectively, these studies show that pre-existing voids serve as important dislocation nucleation sites via the formation of shear loops as the voids collapse under shock. The increased dislocation production coupled with the local increase in energy generates hot spots and localized melting. As experimental capabilities for the temporal and spatial resolution required to understand the microstructural behavior of pre-existing voids under shock loading come of age, molecular dynamics simulations continue to illuminate the localized, nanoscale behavior of void collapse during shock loading.

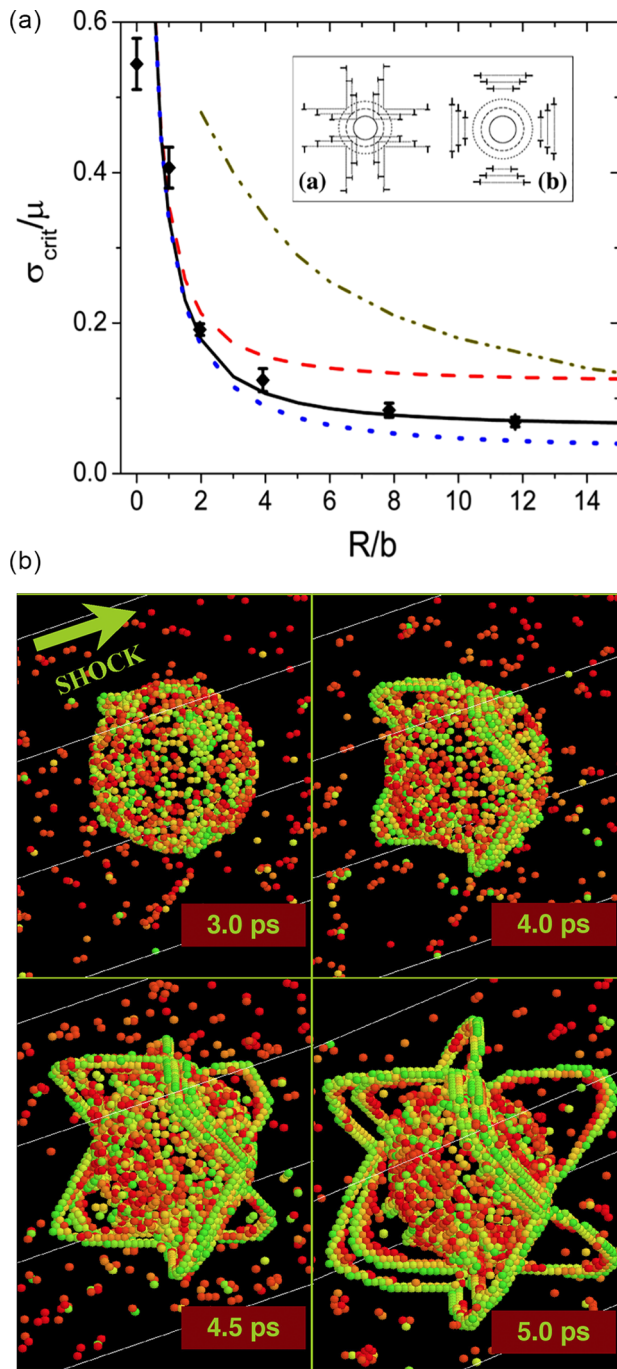


**FIG. 20.** (a) Time evolution in ps for a void with radius 1.5 nm at 8 GPa shock. (b) Calculated stress threshold for dislocation emission normalized by shear modulus as a function of void radius normalized by burgers vector. MD simulations (diamond), model from Reisman *et al.* (dashed-dotted-dotted)<sup>139</sup> and analytical model from Ref. 140 for different dislocation core sizes: b (dashed), 2b (solid), and 4b (dotted). The inset compares the proposed loop mechanisms for void growth. Reproduced with permission from "Atomistic modeling of shock-induced void collapse in copper," *Appl. Phys. Lett.* **86**(16), 161902 (2005). Copyright 2005 AIP Publishing.

### C. Porous materials

By extension, distended materials such as closed-cell porous materials provide significant insights into the role played by pre-existing defects. Cavities within these materials tend to collapse under shock loading, which leads to an intense steepening of the pressure–volume relationship, known also as the Hugoniot curve.<sup>149</sup> For porous Fe and Al, a 1969 theoretical study showed that the Hugoniot for both materials tends to steepen as the porosity increases and eventually flips over for larger porosities.<sup>150</sup> This change, depicted in Fig. 23, is crucial because it indicates that for large porosities, the change in specific volume is significantly altered as the initial shock passes through. By calculating the Hugoniot and examining the integral of the Rayleigh line, an increased energy dissipation during shock in comparison to solids was observed<sup>151,152</sup> due to the shift in the shock Hugoniot, which is the characteristic of porous materials.

Steepening of the Hugoniot curve has been observed via MD simulations of Cu nanofoams with porosity ranging from 18% to 54% under shock loading with piston velocities ranging from 0.5–3.5 km/s.<sup>153</sup> The HEL of Cu has been shown to decrease as porosity increases, and the amount of bulk material between voids affects the emission of dislocations; voids that are closer together tend to have more disordered structures rather than dislocations between them. At higher piston velocities, fewer dislocations are observed to form as the voids collapse via jetting, leading to the development of hot spots when internal jets interact with the rear void surfaces. In essence, this study reiterates the steepening of the Hugoniot for porous material, as shown in Fig. 24, under shock loading via MD simulations while highlighting the formation of shear loops and hot spots during shock loading of porous Cu.<sup>153</sup>

To understand the role of defect geometry and morphology, Zhao *et al.*<sup>154</sup> examined the shock compression of porous Cu via molecular dynamics simulations by implementing a variety of different microstructures into their MD simulations of porous Cu at 0.625 and 2.0 km/s. The initial void shapes and morphologies of porous Cu are shown in Fig. 25(a). The simulated Hugoniot states, given in Fig. 25(b), are in agreement with experiments performed on Cu powders, demonstrating a validation of the Grüneisen equation of state for porous materials.<sup>155</sup> The formation of internal jets was demonstrated at a piston velocity of 2.0 km/s in Fig. 25(c), while at 0.625 km/s, the formation of various dislocation structures is shown in Fig. 25(d). Zhao *et al.*<sup>154</sup> also observed heterogeneous melting and a relationship between shock strength and modes of void collapse. A geometric model demonstrated that collapse occurred via flow along the {111} slip planes, whereas a hydrodynamic mode demonstrated collapse via the formation of nano-jets. The latter case roughened the shock front, forming hot spots and jets at the free surface.<sup>154</sup>

Soulard *et al.*<sup>156</sup> also explored the role of porosity in Cu via MD simulations, exploring voids (both empty and argon-filled) with diameters of 10, 15, and 40 nm mainly at a piston velocity of 1.0 km/s. The pores were arranged randomly in the middle of the sample such that the porosity was limited to 20%. As the shock front moved through the porous region, hot spots were formed and the shock front was slightly reflected, causing the shock strength to decrease as it moved beyond the porous region. They proposed three mechanisms by which the voids collapse; first, the voids induce shock focusing as the front moves around the void. Second, the impact of the front surface of the void on the rear face results in jet formation and leads to an internal

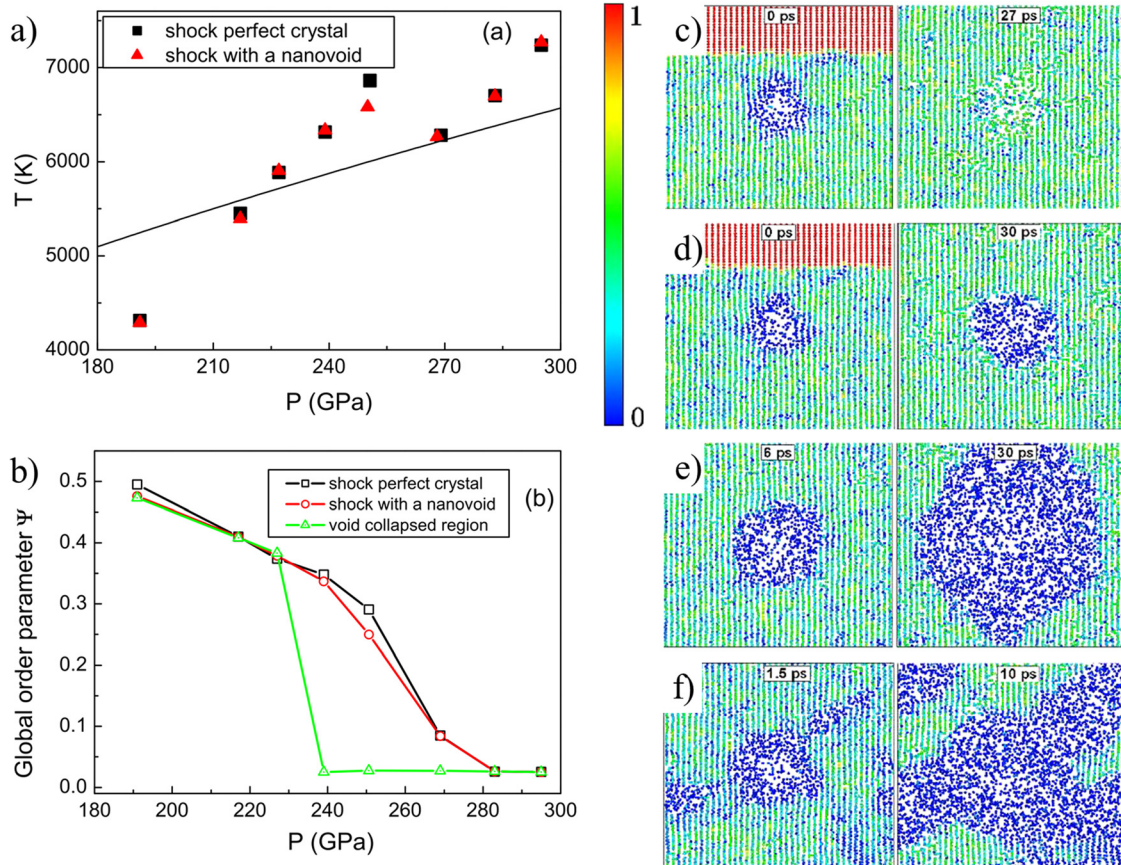


**FIG. 21.** (a) Temperature as a function of pressure. (b) Global order parameter as a function of pressure. (c) Snapshots of nanovoid subject to a piston velocity of 3.1 km/s. (d) Snapshots of nanovoid subject to piston velocity of 3.2 km/s. (e) Snapshots of nanovoid subject to a piston velocity of 3.3 km/s. (f) Snapshots of nanovoid subject to a piston velocity of 3.3 km/s. Reproduced with permission from “Shock melting of single crystal copper with a nanovoid: Molecular dynamics simulations,” *J. Appl. Phys.* **112**(7), 074116 (2012). Copyright 2012 AIP Publishing.

shock.<sup>156</sup> Finally, the emission of dislocations and the associated pore collapse perform plastic work. Soulard *et al.*<sup>156</sup> concluded that plastic work is the predominant process driving shock melting and that the shock intensity, porosity, and void content matter less than the simple presence of the voids themselves. They also emphasized that the complex phenomena around wave interactions and reflections require that the full shock loading history of the sample be known.<sup>156</sup>

The importance of plasticity and void collapse has been reiterated in other materials. In the case of porous Ni, dislocation generation and energy dissipation during void collapse were systematically quantified via MD simulations.<sup>157</sup> Figures 26(a)–26(d) demonstrate the initial microstructures explored throughout this study as well as the dislocation structure following shock compression at a piston velocity of 1.0 km/s. Figure 26(e) shows the energy dissipation over time for each case while Fig. 26(f) displays the dislocation length simultaneously. At the shock velocity of 1.0 km/s, energy dissipation was clearly dominated by dislocation generation, but for greater shock velocities, shock-induced melting became the dominant means of energy dissipation. The void morphology mattered only before voids fully collapsed, but otherwise, only the time-history of energy dissipation was

impacted. As shock intensity increased, void collapse was dominated by internal jetting rather than plasticity.<sup>157</sup>

During void collapse, hot spot formation and plasticity may also lead to the formation of nanograins. Erhart *et al.*<sup>141</sup> performed double-shock experiments on polycrystalline copper with an average grain size of 50  $\mu\text{m}$ ; the first shock generated voids via spall, and then EBSD was performed following a second shock, where the voids were collapsed. Figure 27 shows an EBSD micrograph from a cross section of the double-shocked Cu, demonstrating grain subdivision in the spall plane, where voids were formed during the first shock. The authors note that these results are observed postmortem, so they are limited in understanding how and when grain subdivision occurred.<sup>141</sup> The subdivision of grains in polycrystalline Cu was also observed in recompaction experiments by Jones *et al.*<sup>158</sup> and attributed to the collapse (during second shock) of voids formed by the initial shock. The residual microstructure is hypothesized to have an increased mechanical strength due to the decrease in grain size and defect content.

Erhart *et al.*<sup>141</sup> utilized MD simulations to better understand this phenomenon, but it is impossible to exactly replicate time and length scales of the experiments. This, coupled with a strong dependence on

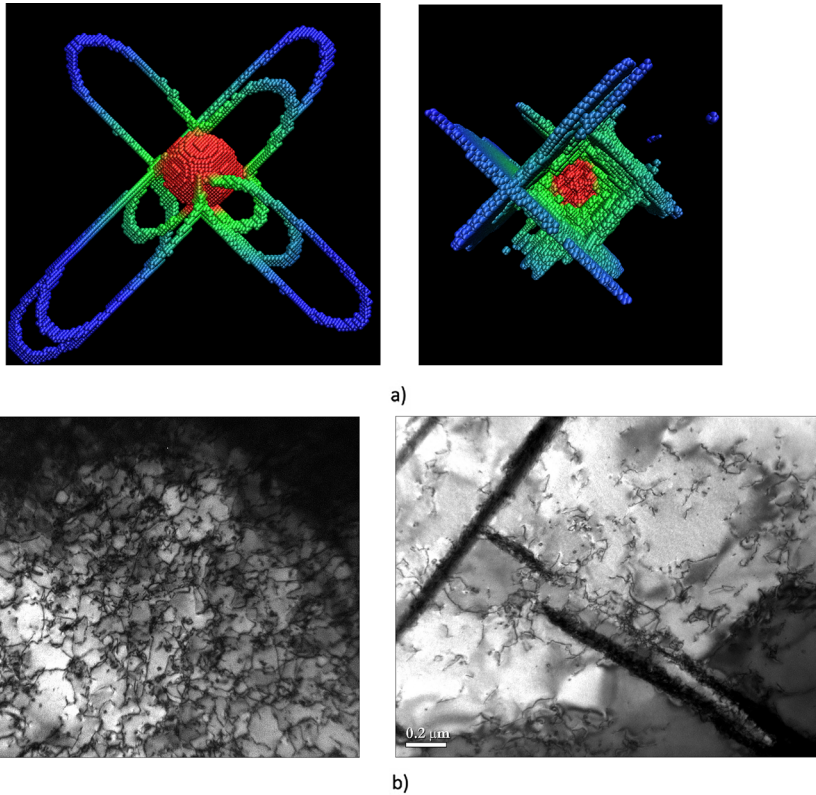


**FIG. 22.** (a) Shear loops emanate from pre-existing voids in Ta under shock loading at strain rates of  $10^8$  (left) and  $10^{10}$   $s^{-1}$  (right) from Tang *et al.*<sup>148</sup> (b) At a strain rate of  $10^9$   $s^{-1}$ , Ta demonstrates deformation via dislocation slip when shocked to 15 GPa (left) and twinning when shocked to 35 GPa (right). Reproduced with permission from Tang *et al.*, *Acta Mater.* **59**(4), 1354–1372 (2011). Copyright 2011 Elsevier.

void size for the critical pressure at which dislocation nucleate and thus void collapse occurs, limits direct simulations due to the extensive void collapse presumed to occur in the experiments. Therefore, instead of simulating Cu, Al was used due to its lower shear modulus and

melting temperatures. MD simulations first performed on Al containing 5% voids shocked from 25 to 100 GPa illustrated the formation of nanograins, shown in the time series in Fig. 28.<sup>141</sup> The top series displays the voids under shock compression as they collapse, forming an

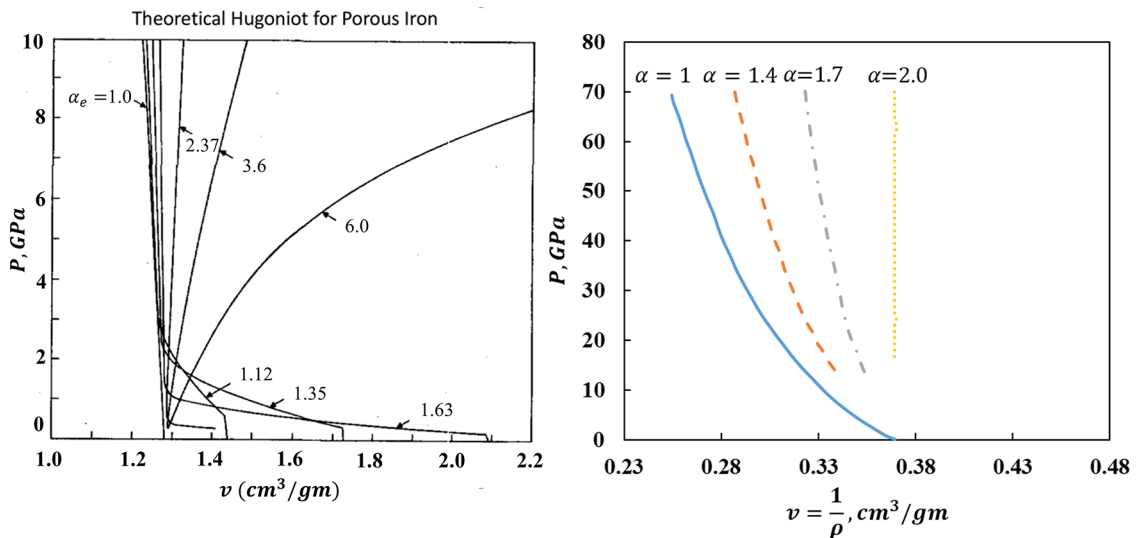


**FIG. 23.** Theoretical Hugoniot curves for porous iron (left) and porous aluminum (right) from Hermann.<sup>150</sup> Reproduced with permission from “Constitutive equation for the dynamic compaction of ductile porous materials,” *J. Appl. Phys.* **40**(6), 2490–2499 (1969). Copyright 1969 AIP Publishing.

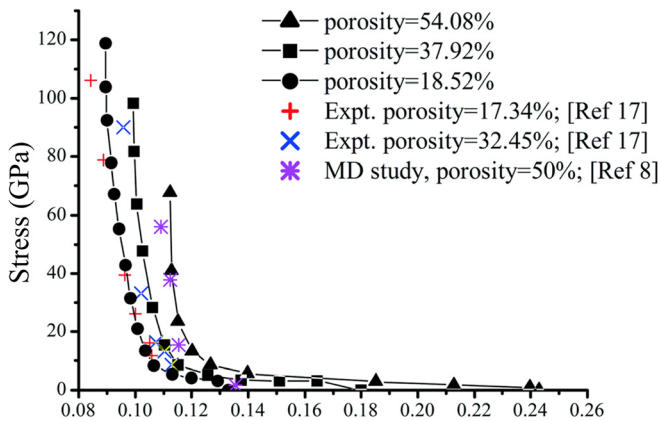


**FIG. 24.** Stress vs specific volume for closed-cell, porous Cu with various porosities. Reproduced with permission from “On shock response of nano-void closed/open cell copper material: Non-equilibrium molecular dynamic simulations,” *J. Appl. Phys.* **115**(1), 013504 (2014). Copyright 2014 AIP Publishing.

intense local plastic region along with a hot spot. The extended porosity of the sample generated extended disordered regions, which seemingly generated nanograins, as shown in the bottom half of Fig. 28. While the results of experiments and simulations are not perfectly matched, the formation of nanograins is apparent and the crucial role of void–void interactions on plasticity is emphasized.<sup>141</sup>

Further MD simulations of nanoporous Al were undertaken by Xiang *et al.*<sup>159</sup> in which several consecutive voids were embedded in an Al single crystal. Void radii were varied in each simulation from 2.0 to 6.0 nm, yielding porosities of 0.4%, 3.4%, and 11.3% (note that the lattice constant is 0.4 nm), respectively. The simulation cell was shocked in the [100] direction at piston velocities of 0.5, 1.0, 2.0, and 4.0 km/s. Results confirmed the formation of hot spots as well as the crucial role of dislocation generation from the surface of the voids, leading to intense, local plastic regions adjacent to the voids. The spall behavior was probed, with measured spall strengths outlined in Table I. With one exception, the spall strength was found to decrease as porosity increased due to the localized temperature increase associated with void collapse. At a piston velocity of 1.0 km/s, the largest

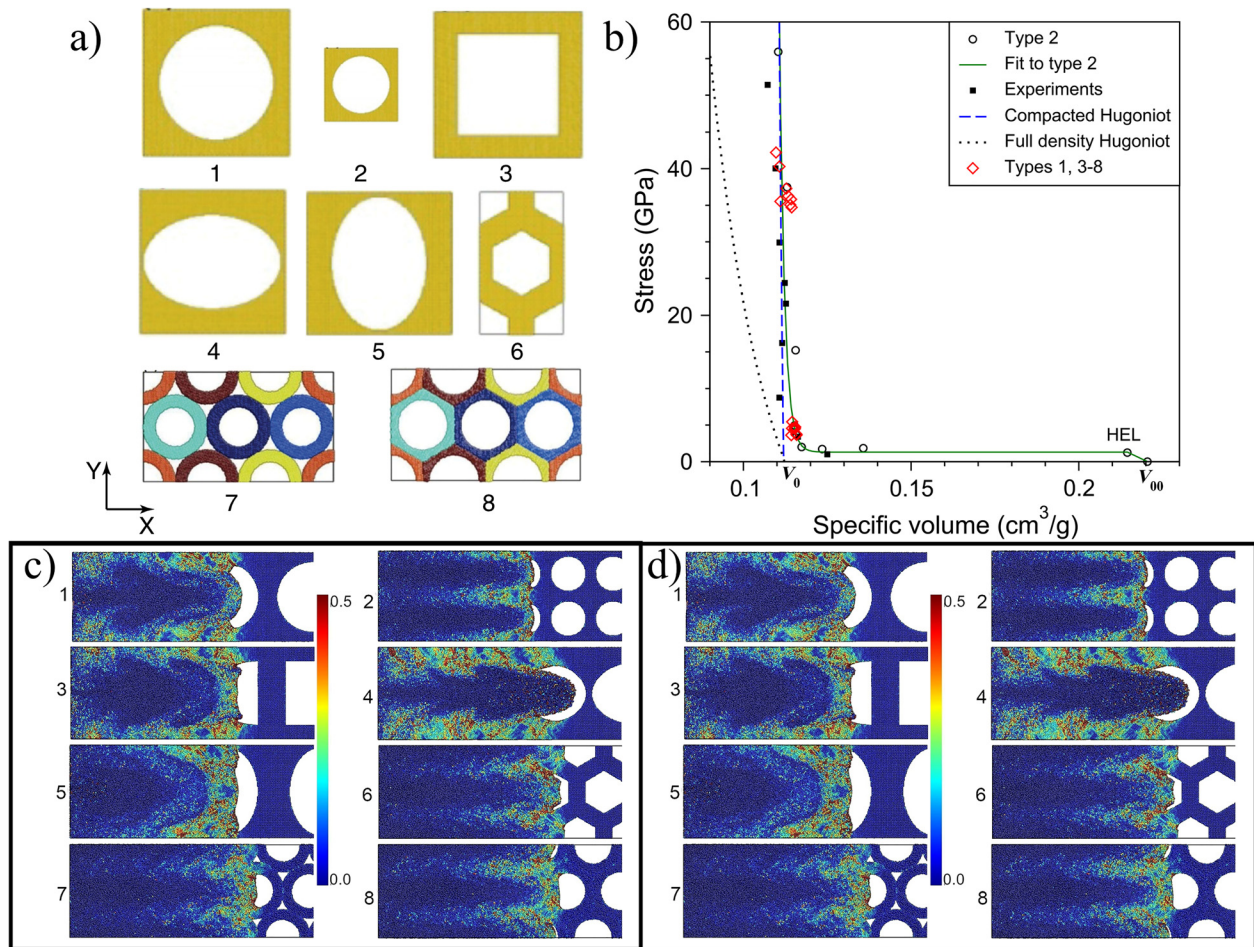


**FIG. 25.** (a) Initial void shapes and morphologies of porous Cu simulations. (b) Stress vs specific volume for different morphologies. (c) Formation of internal jets observed at a piston velocity of 2.0 km/s. (d) Dislocation generation observed at a piston velocity of 0.625 km/s. Reproduced with permission from “Microstructure effects on shock response of Cu nanofoams,” *J. Appl. Phys.* **114**(7), 073501 (2013). Copyright 2013 AIP Publishing.

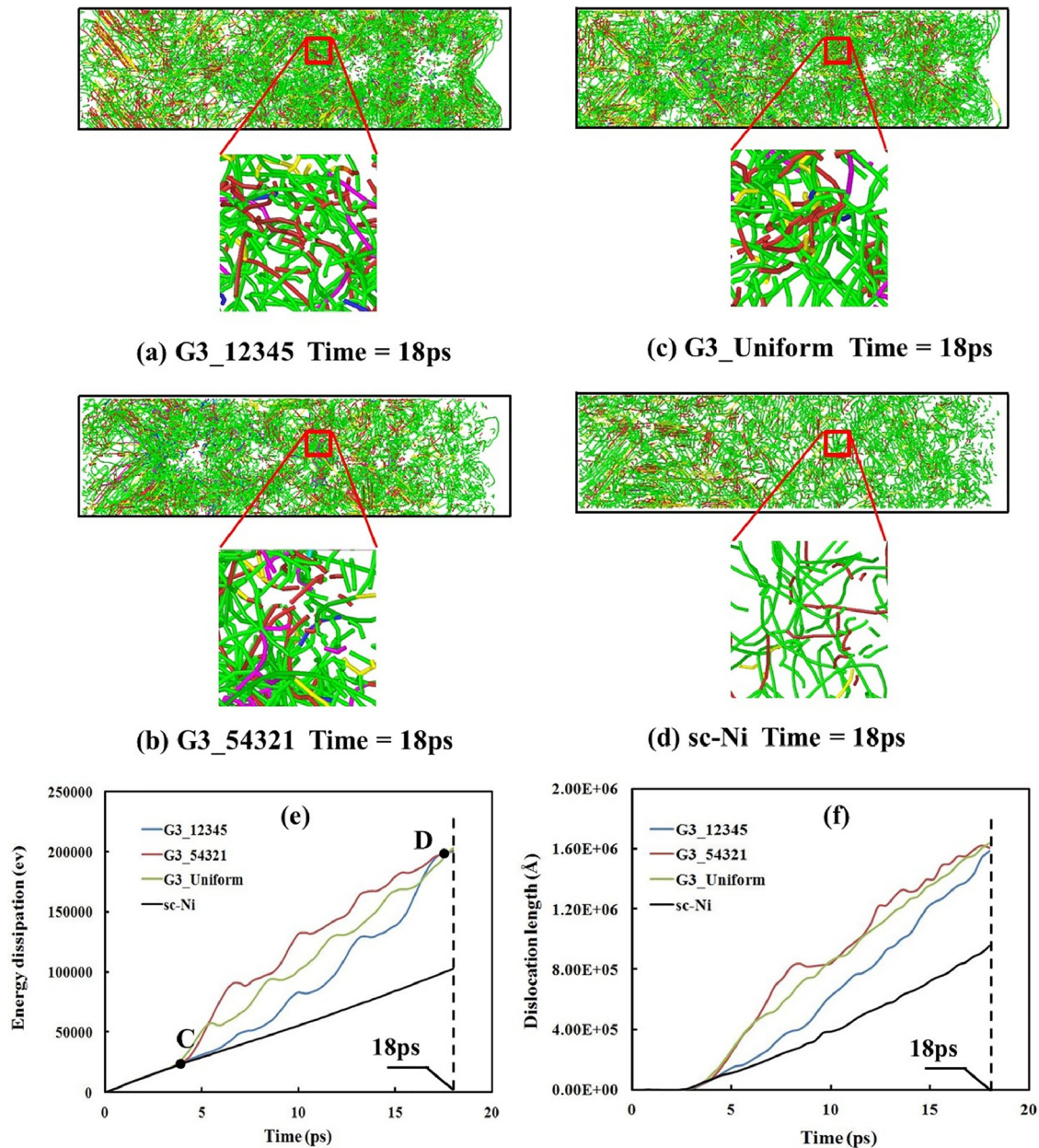


**FIG. 26.** (a) The initial Ni structure with graded voids (top) is subjected to shock loading, and the resulting dislocation structure is highlighted (bottom). The same shock conditions are applied to (b) a sample with uniform voids, (c) a sample with reverse-graded voids, and (d) a single crystal. (e) The energy dissipation and (f) the dislocation generation as functions of time are displayed. Reproduced with permission from Liao *et al.*, *Mech. Mater.* **126**, 13–25 (2018). Copyright 2018 Elsevier.

voids prevented spallation due to the competition between stress attenuation due to minor reflections from the void surfaces and material softening due to local temperature increase.<sup>159</sup>

Void–void interactions and their role in plasticity have been further elucidated by an MD study on the uniaxial compressive deformation of porous Ta.<sup>143</sup> Voids of  $\sim 3.3$  nm radii with an average distance of 10.5 nm were created in a Ta single crystal, generating a void

volume fraction of 4.1%. This sample was subjected to uniaxial peak stresses up to 50 GPa, during which an increase in dislocation activity at a lower applied stress was observed as a result of the multiple voids, demonstrating that void surfaces serve as dislocation sources during deformation. Using the dislocation extraction algorithm (DXA) and common neighbor analysis (CNA), the authors demonstrated agreement for measured dislocation densities for both experiments and a

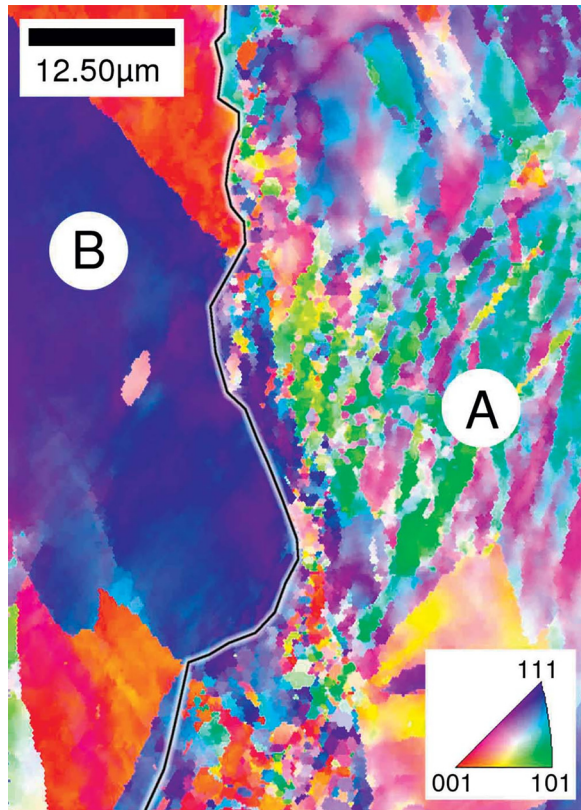


**FIG. 27.** Electron backscatter diffraction (EBSD) orientation map of double-shocked polycrystalline sample where region A, a section of the spall plane, exhibits grain refinement, while region B is representative of the material microstructure outside of the spall plane. Reproduced with permission from Erhart *et al.*, Phys. Rev. B **72**(5), 052104 (2005). Copyright 2005 American Physical Society.

multiscale strength model, as well as agreement with Ashby's theory of geometrically-necessary dislocations (GNDs). Figure 29 summarizes this result, showing that the dislocation density observed via DXA matched calculations of GNDs. While other models identify pore compaction and plasticity as serial phenomena, this study showed that compaction and dislocation generation are instead coupled.<sup>143</sup>

## V. DISCUSSION

In Secs. I–IV, we have evaluated and summarized the existing literature describing the role of material defects and heterogeneities in dictating the shock and spall response of metals. There are three distinct sub-topics at hand, discernable by the methodology through which they have been examined. First, polycrystallinity and grain size play an important role in spalling, with the boundaries often acting as preferential sites for void nucleation and providing easy paths for void growth. Second, inclusions such as second phase particles and precipitates have been studied mainly via experiments, with the most thorough investigations examining the material microstructure before and after shock loading. The third is the role of pre-existing voids, extending into distended media as an extreme case; the majority of investigations are performed via simulations in order to capture the collapse phenomena during shock loading.

Varying grain boundary orientations contributes to material anisotropy during both elastic and plastic deformation, which alters the spall strength due to stress concentrations.<sup>47,48</sup> Deformation twinning and void nucleation are also impacted by grain boundary orientation, including the tendency to nucleate voids for boundary orientation relative to the shock loading direction.<sup>49,50</sup> Preference for deformation via slip or twinning is a function of grain boundary misorientation, with further dependence on crystalline structure.<sup>54–60,62,63</sup> A key reason for interest in polycrystalline materials pertains to conflicts with the Hall–Petch relationship,<sup>71,72</sup> which have been identified in countless studies.<sup>20,58,62,74–78</sup> Localization of stress due to dislocation

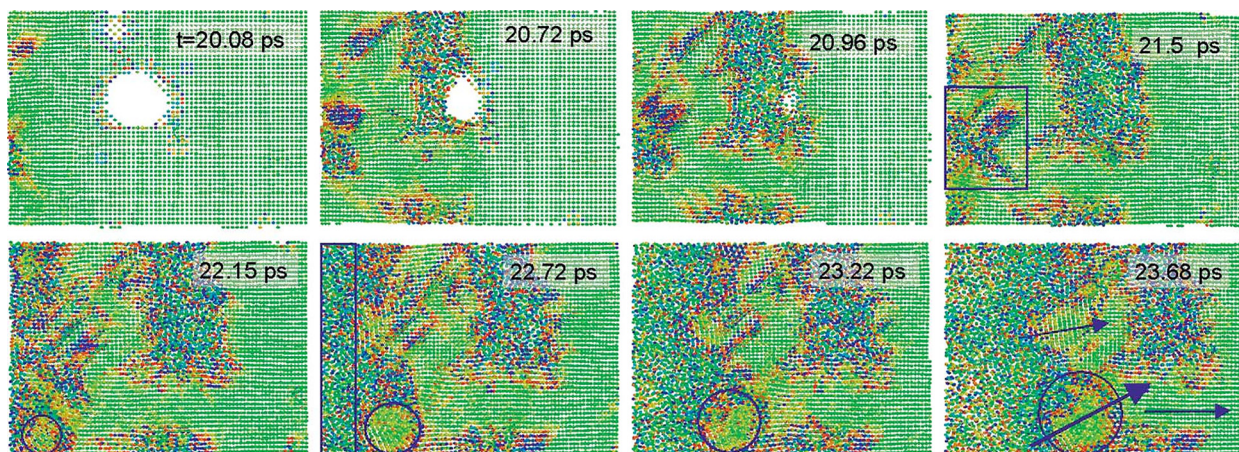


**FIG. 28.** Time series of void collapse in Al under 25 GPa shock loading colored by a centrosymmetry parameter (green represents FCC, while blue and red correspond to non-FCC atoms.) Dislocations are emitted on the  $\{111\} \langle 110 \rangle$  glide system, marked in the frame at 21.5 ps. In the last four snapshots, the circles indicate the formation of nano-grains adjacent to the void. Reproduced with permission from Erhart *et al.*, Phys. Rev. B **72**(5), 052104 (2005). Copyright 2005 American Physical Society.

**TABLE I.** Nanoporous Al is probed via MD simulation, demonstrating a decrease in spall strength and an increase in spall temperature, both as a function of porosity. Reproduced with permission from Xiang *et al.*, *Int. J. Plast.* **97**, 24–45 (2017). Copyright 2017 Elsevier.

$u_p$ (km/s)	$R$	$\sigma_{sp}$ (Gpa)	$T_{sp}$ (K)	$\Delta T_{sp}$ (K)
1.0	0 <sup>a</sup>	9.06	283	454
	5a	9.01	295	494
	10a	8.63	303	588
	15a	... <sup>b</sup>	...	...
2.0	0	9.87	318	221
	5a	9.83	326	381
	10a	9.35	365	579
	15a	8.46	551	647

<sup>a</sup> $R = 0$  represents the sc-Al sample.

<sup>b</sup>In the np-Al sample with  $R = 15a$ , spalling does not occur.

pile ups and other defects may increase the likelihood for certain grain boundaries to be sites of failure<sup>75,76,79</sup> although there are many contradicting studies, so the continued exploration of this matter requires careful, systematic consideration of the phenomena of interest.<sup>58</sup> As grain size is reduced to the nanoscale, results continue to be contradictory, with several reviews already covering the matter thoroughly.<sup>81,86</sup> Interestingly, a quantitative model for high strain rates has been developed to reflect multiple regimes where (1) the Hall–Petch behavior is followed, (2) strength scales inversely to the Hall–Petch law, and (3) grain size no longer matters.<sup>82,83</sup> In addition to grain size, texture also influences spall strength by varying the anisotropy in the material. Forging in iron was shown to increase spall strength due to a decrease in grain size<sup>87</sup> while rolling and annealing iron decreased spall strength by increasing the number of sites available for void nucleation.<sup>89</sup> Studies by Peralta *et al.*<sup>90</sup> and Gray *et al.*<sup>93</sup> emphasize that the processing of materials affects the nucleation, growth, and coalescence of damage by varying the grain size and texture, further complicating our understanding of deformation under shock loading.

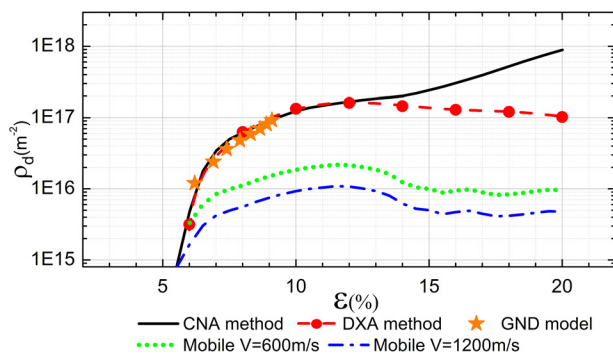


**FIG. 29.** Dislocation density as a function of strain for CNA, DXA, and GND calculations. Reasonable agreement between models is observed although divergence beyond 14% strain is attributed to difference between DXA calculations, which follow trial circuits to calculate dislocation length, and CNA calculations, which utilize a spherical shell. Reproduced with permission from Ruestes *et al.*, *Comput. Mater. Sci.* **88**, 92–102 (2014). Copyright 2014 Elsevier.

For inclusions, several themes have become apparent in the literature. A variety of microstructures and materials have been studied, and the methodology for such studies has not been uniform. The ability to fully isolate and control one specific defect type is nearly impossible via experiments due to the complicated nature of materials processing and preparation. Characterization of the microstructure before shock loading is crucial to understanding the ensuing changes in material behavior. While early studies note the presence of inclusions, they do not quantify or characterize them before shock loading, making it difficult to extend discussion to the role of such impurities.<sup>26,114</sup> More recent studies exemplify means of characterizing the material before shock; for example, a study exploring Cu-24%Ag and Cu-15%Nb uses microscopy to show the vastly differing defect structure in each material as well as the respective *postmortem* samples.<sup>13</sup> Another example is given in a study of the AZ31B-4E Mg alloy, where inclusions are not only identified, but their content is measured.<sup>125</sup> While other studies measure the number of impurities, these studies are exemplary in that their thorough analysis prior to shock loading links to the changes in shock behavior.

The changes in shock behavior due to these inclusions vary on a case-by-case basis. A decrease in HEL was observed for Mg-based materials such as an AZ31B-4E and Al containing B and He inclusions.<sup>125,128,129</sup> Conversely, other materials such as CuAg, CuNb, and a cold-rolled 5083-H321 aluminum alloy,<sup>13,124</sup> in addition to the Cu-Ta system, demonstrate an increase in spall strength as well.<sup>13,120,124</sup> Most other systems experience a decrease in spall strength, naming inclusions as the key reason for such a change, thus necessitating more thorough, focused experimental studies in order to reconcile these differences.<sup>20,23,24,27,128,129</sup> Post-shock recovery shows that the presence of inclusions may lead to a void-nucleation dominated spall process, with voids nucleating at interfaces,<sup>13,24,25,27,120,124,125,127</sup> while other materials demonstrate a failure process dominated by coalescence of voids.<sup>13,24</sup> Ideally, further systematic studies which quantify the concentration and size of voids, as demonstrated in a few works discussed here,<sup>13,25,27</sup> would be a powerful tool for better examining the trends in how strength and void generation are altered by the presence of heterogeneities.

Studies exploring pre-existing voids and distended materials, particularly the role of voids in altering the shock behavior of a material, have been dominated by understanding the formation of hot spots under shock loading rather than direct changes in the HEL and spall strength. Hatano<sup>132</sup> notes that pre-existing voids lead to a decrease in HEL as a function of increasing void radius, but this point must be further investigated. The majority of studies directly discussing pre-existing voids have been performed via simulations, again reiterating the need for continuing the development of experimental analysis tools. The inability to fully understand the process of shock loading with nanoscale time resolution is a major shortcoming of the field,<sup>160</sup> where the complex phenomena of wave interactions and reflections require that the full shock loading history of the sample be known.<sup>156</sup> Specifically, internal jetting, temperature increase, and the asymmetric nature of cavity collapse, as well as the establishment of the complex interactions within a field of cavities, require more accurate, time-resolved measurements of temperature.<sup>144</sup>

Existing studies emphasize the localized behavior of pre-existing voids subjected to shock loading. A sufficiently strong shock generates void collapse, which can occur via two modes. Weaker shocks induce

shear loop emission from the void, generating intense plastic regions adjacent to the collapsing void.<sup>132,148</sup> The stress required for shear loop generation in Cu has been calculated by Davila *et al.*,<sup>140</sup> showing that the well-studied inverse case of void growth via dislocation loop emission<sup>145</sup> parallels that of void collapse for weaker shocks. Dislocation generation can be directly linked to localized temperature increase, but for even stronger shocks, the formation of a localized fluid phase has been observed,<sup>137</sup> which may seemingly lead to void collapse via jetting,<sup>134</sup> emphasizing the importance of understanding the highly localized microscale behaviors as well as the bulk material behavior.<sup>146</sup> Collapse via dislocation emission or jetting both lead to intermolecular collisions as the front surface of the void impacts the rear surface.<sup>133</sup>

Studies exploring distended materials, i.e., foams and powders, serve as an extension of the pre-existing void case since they provide significant insight into the role played by a complex arrangement of defects. Distended materials have been consistently shown to exhibit a steepened Hugoniot curve in comparison to the materials' fully dense counterpart.<sup>149,150,153</sup> While few studies note a decrease in HEL<sup>153</sup> and spall strength,<sup>159</sup> the majority of the work summarized in this review has focused on the formation of hot spots via void collapse. As observed in the case of single pre-existing voids, collapse leads to energy dissipation and to a lack of localized thermal equilibrium.<sup>151,152,161,162</sup> A highly localized microkinetic energy is linked to the geometrically necessary energy added by a void,<sup>152</sup> in turn demonstrating that material heterogeneities may induce shock front roughening via complex reflections from cavities that are simultaneously collapsing.<sup>154,156</sup> The formation of hot spots and jetting is observed in several studies.<sup>141,152–154,156,163</sup> As is the case for singular voids, intense plastic regions due to dislocation emission are observed for porous materials, but an elaborate plastic region forms due to the close proximity of voids in these materials. This has been shown to lead to the formation of nanograins, and in cases, material recrystallization and localized melting.<sup>141</sup> Shock intensity and the mode of void collapse is reiterated, with weaker shocks inducing collapse via shear loop emission and stronger shocks inducing jetting.<sup>141,153,154,159,162</sup> The threshold between these modes, while likely more of a spectrum, has yet to be determined. However, many studies have covered the role of various void morphologies, showing that the formation of a jet is deeply dependent on the void geometry itself.<sup>152,154,162,163</sup> The development of localized plastic regions is also observed in these morphology studies although systematic variance of defect concentration, size, distribution, and depth remain outstanding. A significant body of work has been conducted, and yet the desire to understand the formation of hot spots has dominated the field of voids and distended media, leaving significant room for systematic studies regarding the interplay between dislocation formation and jetting as well as generalization and extension of our knowledge of model materials.

## VI. CONCLUSIONS

The goal of this contribution is to summarize the existing body of literature describing the role of pre-existing heterogeneities such as second phase particles, inclusions, precipitates, and voids on the shock behavior of materials. Our key findings are summarized below:

(1) Few studies specifically isolate the role of pre-existing inclusions, which is known to be challenging, particularly for

experimental studies, but characterization of second phase particles, precipitates, and other inclusions both before and after shock loading can reveal the means by which microstructure alters deformation, thus allowing for more systematic and generalized theories to be formed.

- (2) No generalized trend of increase or decrease in either HEL or spall strength was identified for materials containing pre-existing inclusions, but studies show that the nucleation and growth of voids adjacent to heterogeneities is altered, with some materials nucleating more voids at the interface and others exhibiting an increase in void growth.
- (3) There are few direct measurements of HEL and spall strength thus far on materials containing pre-existing voids and distended materials. Calculation of their Hugoniot curves shows that increasing porosity leads to a steepening of the Hugoniot curve in comparison to fully dense material, generating higher temperatures.
- (4) Studies of pre-existing voids and distended materials emphasize the formation of hot spots due the geometrically necessary excess energy and resultant impact of the front void surface with the rear; under shock loading, void collapse may occur via shear loop emission for weaker shocks or by jetting for stronger shocks. Highly localized plasticity, melting, and excess energy may be present, with void morphology playing and important role in the dominant mechanisms.
- (5) Void collapse via shear loop emission and jetting are coupled phenomena, yet one tends to be more dominant than the other; the threshold between collapses via either mechanism is likely related to the microkinetic energy and depends on localized melting under shock loading.
- (6) For all heterogeneities, continuous improvement toward time-resolved, *in situ* experimental data must be made in order to validate and elucidate upon results gathered from simulations and experiments, which will strengthen the overall ability to understand and predict how materials behave under shock loading.

## ACKNOWLEDGMENTS

The support provided to R. Flanagan and M. Meyers by the Center for Matter in Extreme Conditions (Award No. DENA0003842) is gratefully acknowledged. This work was supported by the U.S. Department of Energy (DOE) through the Los Alamos National Laboratory. The Los Alamos National Laboratory is operated by Triad National Security, LLC, for the National Nuclear Security Administration of the U.S. Department of Energy (Contract No. 89233218CNA000001).

## AUTHOR DECLARATIONS

### Conflict of Interest

The authors have no conflicts to disclose.

### Author Contributions

M.A.M. and S.J.F. proposed the project. R.M.F. prepared the draft and figures. All authors contributed to writing and revision of the paper. We thank Prof. Roger Narayan for the invitation to contribute this review article.

## DATA AVAILABILITY

Data sharing is not applicable to this article as no new data were created or analyzed in this study.

## REFERENCES

- <sup>1</sup>Y. M. Gupta *et al.*, “Large elastic wave amplitude and attenuation in shocked pure aluminum,” *J. Appl. Phys.* **105**(3), 036107 (2009).
- <sup>2</sup>B. Gurrutxaga-Lerma, M. A. Shehadeh, D. S. Balint, D. Dini, L. Chen, and D. E. Eakins, “The effect of temperature on the elastic precursor decay in shock loaded FCC aluminium and BCC iron,” *Int. J. Plast.* **96**, 135–155 (2017).
- <sup>3</sup>M. Sliva *et al.*, “Femtosecond x-ray diffraction studies of the reversal of the microstructural effects of plastic deformation during shock release of tantalum,” *Phys. Rev. Lett.* **120**(26), 265502 (2018).
- <sup>4</sup>R. F. Smith *et al.*, “Time-dependence of the alpha to epsilon phase transformation in iron,” *J. Appl. Phys.* **114**(22), 223507 (2013).
- <sup>5</sup>N. K. Bourne, J. C. F. Millett, and G. T. Gray, “On the shock compression of polycrystalline metals,” *J. Mater. Sci.* **44**(13), 3319–3343 (2009).
- <sup>6</sup>M. A. Meyers, *Dynamic Behavior of Materials* (John Wiley and Sons, 1994).
- <sup>7</sup>S. J. Turneaure, P. Renganathan, J. M. Winey, and Y. M. Gupta, “Twinning and dislocation evolution during shock compression and release of single crystals: Real-time x-ray diffraction,” *Phys. Rev. Lett.* **120**(26), 265503 (2018).
- <sup>8</sup>C. L. Williams, “Structure-property relationships under extreme dynamic environments: Shock recovery experiments,” *Synthesis SEM Lectures on Experimental Mechanics* (Morgan and Claypool, 2019), Vol. 2, No. 1, pp. 1–155.
- <sup>9</sup>D. D. Mallick, C. L. Williams, and J. W. Wilkerson, “A brief review of spall failure in pure and alloyed magnesium,” *J. Dyn. Behav. Mater.* **6**, 423–431 (2020).
- <sup>10</sup>D. E. Grady, “The spall strength of condensed matter,” *J. Mech. Phys. Solids* **36**(3), 353–384 (1988).
- <sup>11</sup>T. P. Remington *et al.*, “Spall strength dependence on grain size and strain rate in tantalum,” *Acta Mater.* **158**, 313–329 (2018).
- <sup>12</sup>S. Fensin, G. Gray, N. Bourne, and R. Hixson, “Microstructure based failure criterion for ductile materials,” *EPJ Web Conf.* **183**, 03005 (2018).
- <sup>13</sup>S. J. Fensin, E. K. Walker, E. K. Cerreta, C. P. Trujillo, D. T. Martinez, and G. T. Gray, “Dynamic failure in two-phase materials,” *J. Appl. Phys.* **118**(23), 235305 (2015).
- <sup>14</sup>D. R. Jones, S. J. Fensin, B. G. Ndefru, D. T. Martinez, C. P. Trujillo, and G. T. Gray III, “Spall fracture in additive manufactured tantalum,” *J. Appl. Phys.* **124**(22), 225902 (2021).
- <sup>15</sup>E. J. Lieberman, R. A. Lebensohn, D. B. Menasche, C. A. Bronkhorst, and A. D. Rollett, “Microstructural effects on damage evolution in shocked copper polycrystals,” *Acta Mater.* **116**, 270–280 (2016).
- <sup>16</sup>T. Antoun, D. R. Curran, L. Seaman, G. I. Kanel, S. V. Razorenov, and A. V. Utkin, *Spall Fracture* (Springer Science and Business Media, 2003).
- <sup>17</sup>A. K. Zurek and M. A. Meyers, “Microstructural aspects of dynamic failure,” in *High-Pressure Shock Compression of Solids II: Dynamic Fracture and Fragmentation*, edited by L. Davison, D. E. Grady, and M. Shahinpoor (Springer, New York, NY, 1996), pp. 25–70.
- <sup>18</sup>D. R. Curran, L. Seaman, and D. A. Shockey, “Dynamic failure of solids,” *Phys. Rep.* **147**(5), 253–388 (1987).
- <sup>19</sup>M. A. Meyers and C. Taylor Aimone, “Dynamic fracture (spalling) of metals,” *Prog. Mater. Sci.* **28**(1), 1–96 (1983).
- <sup>20</sup>R. W. Minich, J. U. Cazamias, M. Kumar, and A. J. Schwartz, “Effect of microstructural length scales on spall behavior of copper,” *Metall. Mater. Trans. A* **35**(9), 2663–2673 (2004).
- <sup>21</sup>R. W. Minich, M. Kumar, A. Schwarz, and J. Cazamias, “Scaling, microstructure and dynamic fracture,” *AIP Conf. Proc.* **845**(1), 642–645 (2006).
- <sup>22</sup>G. T. (Rusty) Gray III, “High-strain-rate deformation: Mechanical behavior and deformation substructures induced,” *Annu. Rev. Mater. Res.* **42**, 285–303 (2012).
- <sup>23</sup>R. S. Hixson, J. N. Johnson, G. T. Gray, and J. D. Price, “Effects of interfacial bonding on spallation in metal-matrix composites,” *AIP Conf. Proc.* **370**(1), 555–558 (1996).
- <sup>24</sup>S. V. Razorenov, G. I. Kanel, B. Herrmann, E. B. Zaretsky, and G. E. Ivanchihina, “Influence of nano-size inclusions on spall fracture of copper single crystals,” *AIP Conf. Proc.* **955**(1), 581–584 (2007).
- <sup>25</sup>S. J. Fensin, J. P. Escobedo, G. T. Gray, B. M. Patterson, C. P. Trujillo, and E. K. Cerreta, “Dynamic damage nucleation and evolution in multiphase materials,” *J. Appl. Phys.* **115**(20), 203516 (2014).
- <sup>26</sup>X. Chen, J. R. Asay, S. K. Dwivedi, and D. P. Field, “Spall behavior of aluminum with varying microstructures,” *J. Appl. Phys.* **99**(2), 023528 (2006).
- <sup>27</sup>J. C. Cheng *et al.*, “Effects of second-phase boron particles on impact response of aluminum,” *Mater. Sci. Eng. A* **793**, 139805 (2020).
- <sup>28</sup>G. I. Kanel, S. V. Razorenov, K. Baumung, and J. Singer, “Dynamic yield and tensile strength of aluminum single crystals at temperatures up to the melting point,” *J. Appl. Phys.* **90**(1), 136–143 (2001).
- <sup>29</sup>G. D. Owen, D. J. Chapman, G. Whiteman, S. M. Stirk, J. C. F. Millett, and S. Johnson, “Spall behaviour of single crystal aluminium at three principal orientations,” *J. Appl. Phys.* **122**(15), 155102 (2017).
- <sup>30</sup>J. Millett, G. Gray, G. Whiteman, S. Fensin, and G. Owen, “The mechanical response of pre-shocked aluminium single crystals,” *EPJ Web Conf.* **183**, 02010 (2018).
- <sup>31</sup>W. D. Turley *et al.*, “Spall response of single-crystal copper,” *J. Appl. Phys.* **123**(5), 055102 (2018).
- <sup>32</sup>A. M. Dongare, B. LaMattina, and A. M. Rajendran, “Atomic scale studies of spall behavior in single crystal Cu,” *Proc. Eng.* **10**, 3636–3641 (2011).
- <sup>33</sup>K. Mackencher, R. R. Valisetty, R. R. Namburu, A. Stukowski, A. M. Rajendran, and A. M. Dongare, “Dislocation evolution and peak spall strengths in single crystal and nanocrystalline Cu,” *J. Appl. Phys.* **119**(4), 044301 (2016).
- <sup>34</sup>G. T. Gray, N. K. Bourne, and J. C. F. Millett, “Shock response of tantalum: Lateral stress and shear strength through the front,” *J. Appl. Phys.* **94**(10), 6430–6436 (2003).
- <sup>35</sup>S. G. Song and G. T. Gray, “Structural interpretation of the nucleation and growth of deformation twins in Zr and Ti. I. Application of the coincidence site lattice (CSL) theory to twinning problems in h.c.p. structures,” *Acta Metall. Mater.* **43**(6), 2325–2337 (1995).
- <sup>36</sup>M. A. Meyers, O. Vöhringer, and V. A. Lubarda, “The onset of twinning in metals: A constitutive description,” *Acta Mater.* **49**(19), 4025–4039 (2001).
- <sup>37</sup>J. M. McNaney, L. M. Hsuing, N. R. Barton, and M. Kumar, “Shock driven twinning in tantalum single crystals,” *AIP Conf. Proc.* **1195**(1), 1127–1130 (2009).
- <sup>38</sup>B. Pang *et al.*, “The defect evolution in shock loaded tantalum single crystals,” *Acta Mater.* **148**, 482–491 (2018).
- <sup>39</sup>C. H. Lu *et al.*, “Laser compression of nanocrystalline tantalum,” *Acta Mater.* **61**(20), 7767–7780 (2013).
- <sup>40</sup>G. Whiteman, J. C. F. Millett, B. Pang, Y.-L. Chiu, and I. P. Jones, “The effects of orientation on the shock induced microstructures of single crystal tantalum,” *AIP Conf. Proc.* **2272**(1), 100022 (2020).
- <sup>41</sup>E. N. Hahn, S. J. Fensin, T. C. Germann, and G. T. Gray, “Orientation dependent spall strength of tantalum single crystals,” *Acta Mater.* **159**, 241–248 (2018).
- <sup>42</sup>Q. An *et al.*, “Shock compression and spallation of single crystal tantalum,” *AIP Conf. Proc.* **1426**(1), 1259–1262 (2012).
- <sup>43</sup>P. Renganathan, J. M. Winey, and Y. M. Gupta, “Shock compression and release of a-axis magnesium single crystals: Anisotropy and time dependent inelastic response,” *J. Appl. Phys.* **121**(3), 035901 (2017).
- <sup>44</sup>J. M. Winey, P. Renganathan, and Y. M. Gupta, “Shock wave compression and release of hexagonal-close-packed metal single crystals: Inelastic deformation of c-axis magnesium,” *J. Appl. Phys.* **117**(10), 105903 (2015).
- <sup>45</sup>C. L. Williams, D. D. Mallick, and J. W. Wilkerson, “A concise note on deformation twinning and spall failure in magnesium at the extremes,” *J. Dyn. Behav. Mater.* **6**(4), 432–444 (2020).
- <sup>46</sup>T. de Rességuier, S. Hemery, E. Lescoupe, P. Villechaise, G. I. Kanel, and S. V. Razorenov, “Spall fracture and twinning in laser shock-loaded single-crystal magnesium,” *J. Appl. Phys.* **121**(16), 165104 (2017).
- <sup>47</sup>S. J. Fensin, S. M. Valone, E. K. Cerreta, and G. T. Gray, “Influence of grain boundary properties on spall strength: Grain boundary energy and excess volume,” *J. Appl. Phys.* **112**(8), 083529 (2012).
- <sup>48</sup>S.-N. Luo, T. C. Germann, D. L. Tonks, and Q. An, “Shock wave loading and spallation of copper bicrystals with asymmetric  $\Sigma 3\langle 110 \rangle$  tilt grain boundaries,” *J. Appl. Phys.* **108**(9), 093526 (2010).

- <sup>49</sup>F. Cao *et al.*, "Orientation dependence of shock-induced twinning and sub-structures in a copper bicrystal," *Acta Mater.* **58**(2), 549–559 (2010).
- <sup>50</sup>S. J. Fensin *et al.*, "Effect of loading direction on grain boundary failure under shock loading," *Acta Mater.* **64**, 113–122 (2014).
- <sup>51</sup>L. Zhang, C. Lu, and K. Tieu, "Atomistic simulation of tensile deformation behavior of  $\Sigma$ 5 tilt grain boundaries in copper bicrystal," *Sci. Rep.* **4**(1), 5919 (2014).
- <sup>52</sup>E. Fortin, B. Shaffer, S. Opie, and P. Peralta, "Nucleation and growth of voids in shock loaded copper bicrystals," *AIP Conf. Proc.* **2272**(1), 120005 (2020).
- <sup>53</sup>E. Fortin, B. Shaffer, S. Opie, M. Catlett, and P. Peralta, "Inter- and transgranular nucleation and growth of voids in shock loaded copper bicrystals," in *Characterization of Minerals, Metals, and Materials* (TMS, Cham, 2019), pp. 97–108.
- <sup>54</sup>S. J. Fensin *et al.*, "Effect of grain boundary structure on plastic deformation during shock compression using molecular dynamics," *Modell. Simul. Mater. Sci. Eng.* **21**(1), 015011 (2012).
- <sup>55</sup>J. P. Escobedo, E. K. Cerreta, and D. Dennis-Koller, "Effect of crystalline structure on intergranular failure during shock loading," *JOM* **66**(1), 156–164 (2014).
- <sup>56</sup>J. Chen, E. N. Hahn, A. M. Dongare, and S. J. Fensin, "Understanding and predicting damage and failure at grain boundaries in BCC Ta," *J. Appl. Phys.* **126**(16), 165902 (2019).
- <sup>57</sup>J. Chen and S. J. Fensin, "Associating damage nucleation and distribution with grain boundary characteristics in Ta," *Scr. Mater.* **187**, 329–334 (2020).
- <sup>58</sup>J. P. Escobedo *et al.*, "Effects of grain size and boundary structure on the dynamic tensile response of copper," *J. Appl. Phys.* **110**(3), 033513 (2011).
- <sup>59</sup>L. Wayne *et al.*, "Statistics of weak grain boundaries for spall damage in polycrystalline copper," *Scr. Mater.* **63**(11), 1065–1068 (2010).
- <sup>60</sup>A. D. Brown *et al.*, "Microstructural effects on damage nucleation in shock-loaded polycrystalline copper," *Metall. Mater. Trans. A* **46**(10), 4539–4547 (2015).
- <sup>61</sup>T. Nguyen, D. J. Luscher, and J. W. Wilkerson, "The role of elastic and plastic anisotropy in intergranular spall failure," *Acta Mater.* **168**, 1–12 (2019).
- <sup>62</sup>E. V. Fortin, A. D. Brown, AD, L. Wayne, and P. D. Peralta, "Microstructural Analysis of Spall Damage Nucleation and Growth in Multicrystalline Titanium," *Proceedings of the ASME 2016 International Mechanical Engineering Congress and Exposition*. Volume 9: Mechanics of Solids, Structures and Fluids; NDE, Diagnosis, and Prognosis. Phoenix, Arizona, USA. November 11–17, 2016. V009T12A044. (ASME, 2016).
- <sup>63</sup>S. J. Fensin, E. K. Cerreta, G. T. G. Iii, and S. M. Valone, "Why are some interfaces in materials stronger than others?," *Sci. Rep.* **4**(1), 5461 (2014).
- <sup>64</sup>M. A. Meyers, H. Jarmakani, E. M. Bringa, and B. A. Remington, "Chapter 89 dislocations in shock compression and release," in *Dislocations in Solids*, edited by J. P. Hirth and L. Kubin (Elsevier, 2009), Vol. 15, pp. 91–197.
- <sup>65</sup>M. A. Meyers, "Thermomechanical processing of a nickel-base superalloy by cold-rolling and shock-wave deformation," Ph.D. thesis (University of Denver, 1974).
- <sup>66</sup>M. A. Meyers, "A 'wavy wave' model for the shocking of polycrystalline metal," in *Proceedings of the 5th International Conference on High Energy Rate Fabrication*, June (1975).
- <sup>67</sup>M. A. Meyers, "A model for elastic precursor waves in the shock loading of polycrystalline metals," *Mater. Sci. Eng.* **30**(2), 99–111 (1977).
- <sup>68</sup>M. A. Meyers and M. S. Carvalho, "Shock-front irregularities in polycrystalline metals," *Mater. Sci. Eng.* **24**(1), 131–135 (1976).
- <sup>69</sup>E. M. Bringa, A. Caro, M. Victoria, and N. Park, "The atomistic modeling of wave propagation in nanocrystals," *JOM* **57**(9), 67–70 (2005).
- <sup>70</sup>O. E. Jones and J. R. Holland, "Effects of grain size on dynamic yielding in explosively loaded mild steel," *Acta Metall.* **16**(8), 1037–1045 (1968).
- <sup>71</sup>E. O. Hall, "The deformation and ageing of mild steel. III. Discussion of results," *Proc. Phys. Soc. B* **64**(9), 747–753 (1951).
- <sup>72</sup>N. J. Petch, "The cleavage strength of polycrystals," *J. Iron Steel Inst.* **174**, 25–28 (1953).
- <sup>73</sup>M. A. Meyers, R. W. Armstrong, and H. O. K. Kirchner, *Mechanics and Materials: Fundamentals and Linkages* (Wiley, 1999).
- <sup>74</sup>M. Cheng, C. Li, M. X. Tang, L. Lu, Z. Li, and S. N. Luo, "Intragranular void formation in shock-spalled tantalum: Mechanisms and governing factors," *Acta Mater.* **148**, 38–48 (2018).
- <sup>75</sup>J. P. Escobedo, E. K. Cerreta, D. Dennis-Koller, C. P. Trujillo, and C. A. Bronkhorst, "Influence of boundary structure and near neighbor crystallographic orientation on the dynamic damage evolution during shock loading," *Philos. Mag.* **93**(7), 833–846 (2013).
- <sup>76</sup>E. K. Cerreta *et al.*, "Early stage dynamic damage and the role of grain boundary type," *Scr. Mater.* **66**(9), 638–641 (2012).
- <sup>77</sup>W. R. Thissell *et al.*, "The effect of material cleanliness on dynamic damage evolution in 10100 Cu," *AIP Conf. Proc.* **620**(1), 475–478 (2002).
- <sup>78</sup>D. Dennis-Koller *et al.*, "Controlled shock loading conditions for microstructural correlation of dynamic damage behavior," *AIP Conf. Proc.* **1426**(1), 1325–1330 (2012).
- <sup>79</sup>A. D. Brown, Q. Pham, E. V. Fortin, P. D. Peralta, B. M. Patterson, J. P. Escobedo-Diaz, E. K. Cerreta, S. N. Luo, D. Dennis-Koller, D. Byler, A. Koskelo., and X. Xiao, "Correlations among void shape distributions, dynamic damage mode and loading kinetics," *JOM* **69**(2), 198–206 (2017).
- <sup>80</sup>A. D. Brown *et al.*, "Correlations between spall damage mode preference and microstructure in shocked polycrystalline copper: A 3D x-ray tomography study," *J. Dyn. Behav. Mater.* **1**(4), 388–396 (2015).
- <sup>81</sup>M. A. Meyers, A. Mishra, and D. J. Benson, "Mechanical properties of nanocrystalline materials," *Prog. Mater. Sci.* **51**(4), 427–556 (2006).
- <sup>82</sup>A. Molinari and T. W. Wright, "A physical model for nucleation and early growth of voids in ductile materials under dynamic loading," *J. Mech. Phys. Solids* **53**(7), 1476–1504 (2005).
- <sup>83</sup>F. Louchet, J. Weiss, and T. Richeton, "Hall-Petch law revisited in terms of collective dislocation dynamics," *Phys. Rev. Lett.* **97**(7), 075504 (2006).
- <sup>84</sup>E. M. Bringa *et al.*, "Ultrahigh strength in nanocrystalline materials under shock loading," *Science* **309**(5742), 1838–1841 (2005).
- <sup>85</sup>D. Tramontina *et al.*, "Molecular dynamics simulations of shock-induced plasticity in tantalum," *High Energy Density Phys.* **10**, 9–15 (2014).
- <sup>86</sup>E. N. Hahn and M. A. Meyers, "Grain-size dependent mechanical behavior of nanocrystalline metals," *Mater. Sci. Eng. A* **646**, 101–134 (2015).
- <sup>87</sup>S. V. Razorenov, G. I. Kanel, A. S. Savinykh, and V. E. Fortov, "Large tensions and strength of iron in different structure states," *AIP Conf. Proc.* **845**(1), 650–653 (2006).
- <sup>88</sup>E. B. Zaretsky and G. I. Kanel, "Yield stress, polymorphic transformation, and spall fracture of shock-loaded iron in various structural states and at various temperatures," *J. Appl. Phys.* **117**(19), 195901 (2015).
- <sup>89</sup>E. B. Zaretsky and G. I. Kanel, "Tantalum and vanadium response to shock-wave loading at normal and elevated temperatures. Non-monotonous decay of the elastic wave in vanadium," *J. Appl. Phys.* **115**(24), 243502 (2014).
- <sup>90</sup>P. Peralta *et al.*, "Characterization of incipient spall damage in shocked copper multicrystals," *Int. J. Damage Mech.* **18**, 393–413 (2008).
- <sup>91</sup>J. T. Lloyd, J. D. Clayton, R. Becker, and D. L. McDowell, "Simulation of shock wave propagation in single crystal and polycrystalline aluminum," *Int. J. Plast.* **60**, 118–144 (2014).
- <sup>92</sup>J. D. Clayton, "Modeling dynamic plasticity and spall fracture in high density polycrystalline alloys," *Int. J. Solids Struct.* **42**(16), 4613–4640 (2005).
- <sup>93</sup>G. T. Gray *et al.*, "Structure/property (constitutive and spallation response) of additively manufactured 316L stainless steel," *Acta Mater.* **138**, 140–149 (2017).
- <sup>94</sup>D. D. Mallick *et al.*, "Laser-driven flyers and nanosecond-resolved velocimetry for spall studies in thin metal foils," *Exp. Mech.* **59**(5), 611–628 (2019).
- <sup>95</sup>D. R. Jones, B. M. Morrow, C. P. Trujillo, G. T. Gray, and E. K. Cerreta, "The  $\alpha$ - $\omega$  phase transition in shock-loaded titanium," *J. Appl. Phys.* **122**(4), 045902 (2017).
- <sup>96</sup>T. de Ressaiguier and M. Hallouin, "Effects of the  $\alpha$ - $\epsilon$  phase transition on wave propagation and spallation in laser shock-loaded iron," *Phys. Rev. B* **77**(17), 174107 (2008).
- <sup>97</sup>N. Amadou, T. de Resseguier, A. Dragon, and E. Brambrink, "Coupling between plasticity and phase transition in shock- and ramp-compressed single-crystal iron," *Phys. Rev. B* **98**(2), 024104 (2018).
- <sup>98</sup>T. W. J. de Geus, R. H. J. Peerlings, and M. G. D. Geers, "Competing damage mechanisms in a two-phase microstructure: How microstructure and loading conditions determine the onset of fracture," *Int. J. Solids Struct.* **97–98**, 687–698 (2016).
- <sup>99</sup>C. Li *et al.*, "Effects of structural anisotropy on deformation and damage of a duplex stainless steel under high strain rate loading," *Mater. Sci. Eng. A* **705**, 265–272 (2017).

- <sup>100</sup>Y. Yang *et al.*, “Effects of the phase interface on initial spallation damage nucleation and evolution in dual phase titanium alloy,” *Mater. Sci. Eng. A* **731**, 385–393 (2018).
- <sup>101</sup>E. M. Bringa, S. Traiviratana, and M. A. Meyers, “Void initiation in FCC metals: Effect of loading orientation and nanocrystalline effects,” *Acta Mater.* **58**(13), 4458–4477 (2010).
- <sup>102</sup>D. D. Koller *et al.*, “Influence of shock-wave profile shape on dynamically induced damage in high-purity copper,” *J. Appl. Phys.* **98**(10), 103518 (2005).
- <sup>103</sup>G. T. Gray III, N. K. Bourne, B. L. Henrie, and J. C. F. Millett, “Influence of shock-wave profile shape (triangular- ‘Taylor-wave’ versus square-topped) on the spallation response of 316L stainless steel,” *J. Phys. IV France* **110**, 773–778 (2003).
- <sup>104</sup>S.-N. Luo, T. C. Germann, and D. L. Tonks, “Spall damage of copper under supported and decaying shock loading,” *J. Appl. Phys.* **106**(12), 123518 (2009).
- <sup>105</sup>J. N. Johnson, G. T. Gray III, and N. K. Bourne, “Effect of pulse duration and strain rate on incipient spall fracture in copper,” *J. Appl. Phys.* **86**(9), 4892 (2020).
- <sup>106</sup>D. R. Jones, S. J. Fensin, D. T. Martinez, C. P. Trujillo, and G. T. Gray, “Effect of peak stress and tensile strain-rate on spall in tantalum,” *J. Appl. Phys.* **124**(8), 085901 (2018).
- <sup>107</sup>E. N. Hahn, T. C. Germann, R. Ravelo, J. E. Hammerberg, and M. A. Meyers, “On the ultimate tensile strength of tantalum,” *Acta Mater.* **126**, 313–328 (2017).
- <sup>108</sup>G. Hillel, L. Meshi, S. Kalabukhov, N. Frage, and E. B. Zaretsky, “Shock wave characterization of precipitate strengthening of PH 13–8 Mo stainless steel,” *Acta Mater.* **187**, 176–185 (2020).
- <sup>109</sup>E. B. Zaretsky and G. I. Kanel, “Abnormal temperature effects on the dynamic yield stress of alpha-brass,” *J. Appl. Phys.* **124**(4), 045902 (2018).
- <sup>110</sup>E. B. Zaretsky, N. Frage, and S. Kalabukhov, “Shock wave determination of the strengthening of commercial aluminum alloy 6061 by point defects,” *Mater. Sci. Eng. A* **761**, 138066 (2019).
- <sup>111</sup>M. A. Meyers and M. A. Dynamic *Behavior of Materials* (J. Wiley, 1994).
- <sup>112</sup>N. K. Bourne, D. Jones, S. Fensin, C. Trujillo, D. Martinez, and G. T. Gray, “On the dynamic tensile strength of an FCC metal,” *AIP Conf. Proc.* **1979**(1), 070007 (2018).
- <sup>113</sup>G. I. Kanel, “Spall fracture: Methodological aspects, mechanisms and governing factors,” *Int. J. Fract.* **163**(1), 173–191 (2010).
- <sup>114</sup>L. E. Murr and J. V. Foltz, “Shock deformation of Inconel 600 alloy: Effect of fine coherent precipitates on explosive-shock hardening,” *J. Appl. Phys.* **40**(9), 3796–3802 (1969).
- <sup>115</sup>R. Becker, “Direct numerical simulation of ductile spall failure,” *Int. J. Fract.* **208**(1), 5–26 (2017).
- <sup>116</sup>R. Becker and K. Callaghan, “Void growth dependence on loading path and mean stress from large-scale numerical simulations,” *Int. J. Plast.* **134**, 102780 (2020).
- <sup>117</sup>R. Becker and K. Callaghan, “Evaluation of Gurson yield function dependencies through large-scale void growth simulations,” *Int. J. Fract.* **209**(1), 235–240 (2018).
- <sup>118</sup>G. T. Gray III, “Shock-loading response of advanced materials,” *AIP Conf. Proc.* **309**(1), 1161 (1994).
- <sup>119</sup>W. Z. Han *et al.*, “Deformation and failure of shocked bulk Cu–Nb nanolaminates,” *Acta Mater.* **63**, 150–161 (2014).
- <sup>120</sup>J. Chen, M. A. Tschopp, and A. M. Dongare, “Role of nanoscale Cu/Ta interfaces on the shock compression and spall failure of nanocrystalline Cu/Ta systems at the atomic scales,” *J. Mater. Sci.* **53**(8), 5745–5765 (2018).
- <sup>121</sup>J. Chen, S. N. Mathaudhu, N. Thadhani, and A. M. Dongare, “Unraveling the role of interfaces on the spall failure of Cu/Ta multilayered systems,” *Sci. Rep.* **10**(1), 208 (2020).
- <sup>122</sup>Y. Yang, C. Wang, X. Chen, K. Chen, H. Hu, and Y. Fu, “The void nucleation mechanism within lead phase during spallation of leaded brass,” *Philos. Mag.* **98**(21), 1975–1990 (2018).
- <sup>123</sup>J. C. Huang and G. T. Gray, “Influence of precipitates on the mechanical response and substructure evolution of shock-loaded and quasi-statically deformed Al–Li–Cu alloys,” *Metall. Trans. A* **20**, 1061–1075 (1989).
- <sup>124</sup>See <https://link.springer.com/article/10.1007%2Fs40870-016-0082-2> for “The role of second phase intermetallic particles on the spall failure of 5083 aluminum” (last accessed August 25, 2020).
- <sup>125</sup>L. Farbaniec, C. L. Williams, L. Kecskes, K. T. Ramesh, and R. Becker, “Microstructural effects on the spall properties of ECAE-processed AZ31B magnesium alloy,” *Int. J. Impact Eng.* **98**, 34–41 (2016).
- <sup>126</sup>See <https://www.sciencedirect.com/science/article/pii/S0022369778900793?via%3Dihub> for “Temperature dependent spall threshold of four metal alloys” (last accessed December 22, 2020).
- <sup>127</sup>N. M. Krywopusk, C. L. Williams, L. J. Kecskes, and T. P. Weihs, “Characterization of spalled AZ31B processed by ECAE,” *Mater. Sci. Eng. A* **767**, 138298 (2019).
- <sup>128</sup>B. Glam, M. Strauss, S. Eliezer, and D. Moreno, “Shock compression and spall formation in aluminum containing helium bubbles at room temperature and near the melting temperature: Experiments and simulations,” *Int. J. Impact Eng.* **65**, 1–12 (2014).
- <sup>129</sup>B. Glam, S. Eliezer, D. Moreno, L. Perelmutter, M. Sudai, and D. Eliezer, “Dynamic fracture and spall in aluminum with helium bubbles,” *Int. J. Fract.* **163**(1–2), 217–224 (2010).
- <sup>130</sup>A. M. Dongare, “Challenges to model the role of heterogeneities on the shock response and spall failure of metallic materials at the mesoscales,” *J. Mater. Sci.* **55**(8), 3157–3166 (2020).
- <sup>131</sup>A. M. Dongare, “Quasi-coarse-grained dynamics: Modelling of metallic materials at mesoscales,” *Philos. Mag.* **94**(34), 3877–3897 (2014).
- <sup>132</sup>T. Hatano, “Dislocation nucleation in shocked FCC solids: Effects of temperature and pre-existing voids,” *Phys. Rev. Lett.* **93**(8), 085501 (2004).
- <sup>133</sup>T. Hatano, “Spatiotemporal behavior of void collapse in shocked solids,” *Phys. Rev. Lett.* **92**(1), 015503 (2004).
- <sup>134</sup>B. L. Holian, T. C. Germann, J.-B. Maillet, and C. T. White, “Atomistic mechanism for hot spot initiation,” *Phys. Rev. Lett.* **89**(28), 285501 (2002).
- <sup>135</sup>J. W. Mintmire, D. H. Robertson, and C. T. White, “Molecular-dynamics simulations of void collapse in shocked model-molecular solids,” *Phys. Rev. B* **49**(21), 14859–14864 (1994).
- <sup>136</sup>D. H. Tsai and R. W. Armstrong, “Defect-enhanced structural relaxation mechanism for the evolution of hot spots in rapidly compressed crystals,” *J. Phys. Chem.* **98**(43), 10997–11000 (1994).
- <sup>137</sup>L. Phillips, R. S. Sinkovits, E. S. Oran, and J. P. Boris, “The interaction of shocks and defects in Lennard-Jones crystals,” *J. Phys.: Condens. Matter* **5**(35), 6357–6376 (1993).
- <sup>138</sup>F. A. Bandak, D. H. Tsai, R. W. Armstrong, and A. S. Douglas, “Formation of nanodislocation dipoles in shock-compressed crystals,” *Phys. Rev. B* **47**(18), 11681–11687 (1993).
- <sup>139</sup>D. B. Reisman, W. G. Wolfer, A. Elsholz, and M. D. Furnish, “Isentropic compression of irradiated stainless steel on the Z accelerator,” *J. Appl. Phys.* **93**(11), 8952–8957 (2003).
- <sup>140</sup>L. P. Dávila *et al.*, “Atomistic modeling of shock-induced void collapse in copper,” *Appl. Phys. Lett.* **86**(16), 161902 (2005).
- <sup>141</sup>P. Erhart, E. M. Bringa, M. Kumar, and K. Albe, “Atomistic mechanism of shock-induced void collapse in nanoporous metals,” *Phys. Rev. B* **72**(5), 052104 (2005).
- <sup>142</sup>C. J. Ruestes *et al.*, “Atomistic simulation of the mechanical response of a nanoporous body-centered cubic metal,” *Scr. Mater.* **68**(10), 817–820 (2013).
- <sup>143</sup>C. J. Ruestes, E. M. Bringa, A. Stukowski, J. F. Rodríguez Nieva, Y. Tang, and M. A. Meyers, “Plastic deformation of a porous BCC metal containing nanometer sized voids,” *Comput. Mater. Sci.* **88**, 92–102 (2014).
- <sup>144</sup>N. K. Bourne, “On the collapse of cavities,” *Shock Waves* **11**(6), 447–455 (2002).
- <sup>145</sup>V. A. Lubarda, M. S. Schneider, D. H. Kalantar, B. A. Remington, and M. A. Meyers, “Void growth by dislocation emission,” *Acta Mater.* **52**(6), 1397–1408 (2004).
- <sup>146</sup>A. M. He, S. Duan, J.-L. Shao, P. Wang, and C. Qin, “Shock melting of single crystal copper with a nanovoid: Molecular dynamics simulations,” *J. Appl. Phys.* **112**(7), 074116 (2012).
- <sup>147</sup>R. M. Flanagan, E. N. Hahn, T. C. Germann, M. A. Meyers, and S. J. Fensin, “Molecular dynamics simulations of ejecta formation in helium-implanted copper,” *Scr. Mater.* **178**, 114–118 (2020).

- <sup>148</sup>Y. Tang, E. M. Bringa, B. A. Remington, and M. A. Meyers, "Growth and collapse of nanovoids in tantalum monocrystals," *Acta Mater.* **59**(4), 1354–1372 (2011).
- <sup>149</sup>M. M. Carroll and A. C. Holt, "Steady waves in ductile porous solids," *J. Appl. Phys.* **44**(10), 4388–4392 (1973).
- <sup>150</sup>W. Herrmann, "Constitutive equation for the dynamic compaction of ductile porous materials," *J. Appl. Phys.* **40**(6), 2490–2499 (1969).
- <sup>151</sup>V. Nesterenko, *Dynamics of Heterogeneous Materials* (Springer Science and Business Media, 2013).
- <sup>152</sup>D. J. Benson, V. F. Nesterenko, F. Jonsdottir, and M. A. Meyers, "Quasistatic and dynamic regimes of granular material deformation under impulse loading," *J. Mech. Phys. Solids* **45**(11), 1955–1999 (1997).
- <sup>153</sup>A. Neogi and N. Mitra, "On shock response of nano-void closed/open cell copper material: Non-equilibrium molecular dynamic simulations," *J. Appl. Phys.* **115**(1), 013504 (2014).
- <sup>154</sup>F. P. Zhao, H. A. Wu, and S. N. Luo, "Microstructure effects on shock response of Cu nanofoams," *J. Appl. Phys.* **114**(7), 073501 (2013).
- <sup>155</sup>F. P. Zhao, Q. An, B. Li, H. A. Wu, W. A. Goddard, and S. N. Luo, "Shock response of a model structured nanofoam of Cu," *J. Appl. Phys.* **113**(6), 063516 (2013).
- <sup>156</sup>L. Soulard, N. Pineau, J. Cl rouin, and L. Colombet, "Molecular dynamics simulations of shock compressed heterogeneous materials. I. The porous case," *J. Appl. Phys.* **117**(11), 115901 (2015).
- <sup>157</sup>Y. Liao, M. Xiang, G. Li, K. Wang, X. Zhang, and J. Chen, "Molecular dynamics studies on energy dissipation and void collapse in graded nanoporous nickel under shock compression," *Mech. Mater.* **126**, 13–25 (2018).
- <sup>158</sup>D. R. Jones, S. J. Fensin, B. M. Morrow, D. T. Martinez, and R. S. Hixson, "Shock recompaction of spall damage," *J. Appl. Phys.* **127**(24), 245901 (2020).
- <sup>159</sup>M. Xiang *et al.*, "Shock responses of nanoporous aluminum by molecular dynamics simulations," *Int. J. Plast.* **97**, 24–45 (2017).
- <sup>160</sup>W. H. Gourdin, "Dynamic consolidation of metal powders," *Prog. Mater. Sci.* **30**(1), 39–80 (1986).
- <sup>161</sup>See <https://www.osti.gov/etdeweb/biblio/7324872> for "Electrical effects at shock loading of metal contacts" (last accessed July 28, 2020).
- <sup>162</sup>Y. Liao, M. Xiang, X. Zeng, and J. Chen, "Molecular dynamics studies of the roles of microstructure and thermal effects in spallation of aluminum," *Mech. Mater.* **84**, 12–27 (2015).
- <sup>163</sup>S. R. Cooper, D. J. Benson, and V. F. Nesterenko, "A numerical exploration of the role of void geometry on void collapse and hot spot formation in ductile materials," *Int. J. Plast.* **16**(5), 525–540 (2000).